AD-A034 075 NORTH CAROLINA STATE UNIV RALEIGH DEPT OF MECHANICAL--ETC F/G 1/3
AN EXPERIMENTAL INVESTIGATION OF FAVORABLE INTERFERENCE EFFECTS--ETC(U)
1976 S L GRIFFITH DAHC04-75-C-0023

UNCLASSIFIED NL

| OF |
AD
A034075

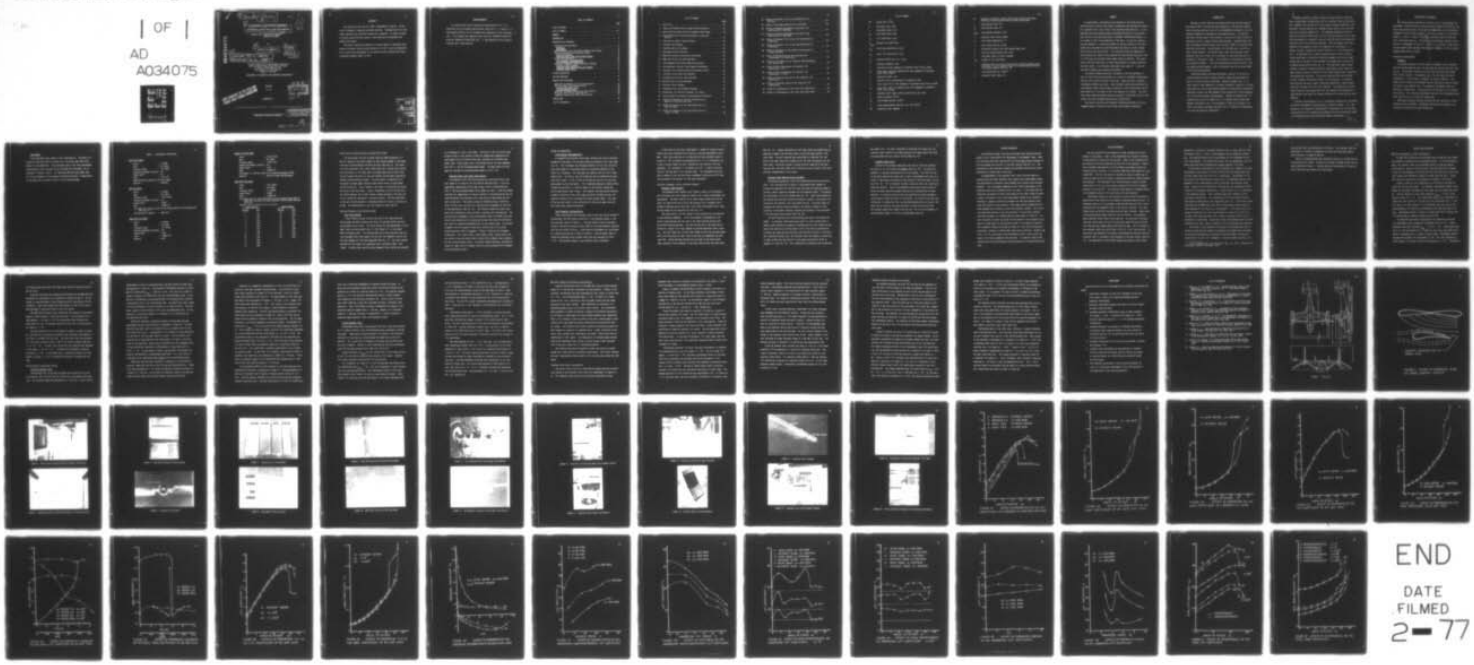

END
DATE
FILMED
2-77

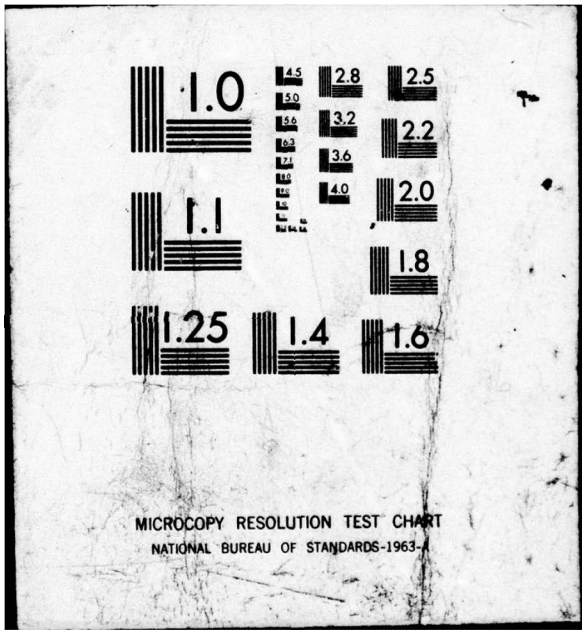
1.0
1.1
1.25
1.4
1.6
1.8
2.0
2.2
2.5
2.8
3.2
3.6
4.0
4.5
5.0
5.6
6.3
7.1
MICROCOPY RESOLUTION TEST CHART
NATIONAL BUREAU OF STANDARDS-1963-A

(9) Master's Thesis

(6) AN EXPERIMENTAL INVESTIGATION OF FAVORABLE INTERFERENCE EFFECTS FROM A WING AND PROPROTOR.

(1) B.S.

Contract Nos. DAHC-04-74-G-0007 NEW
DAHC-04-75-C-0023

by

(10) STEVEN LYTTLE GRIFFITH

(11) 1976

(12) 67 p.

(15) DAHC04-75-C-0023,
DAHC04-75-G-0007

A thesis submitted to the Graduate Faculty of
North Carolina State University at Raleigh
in partial fulfillment of the
requirements for the Degree of
Master of Science

DEPARTMENT OF MECHANICAL AND AEROSPACE ENGINEERING

RALEIGH

1976

APPROVED BY:

Chairman of Advisory Committee

400 714 VB

BIOGRAPHY

The author was born June 21, 1950, in Waynesboro, Virginia. He has lived in Delaware, Tennessee and North Carolina. The majority of his high school education was received in Nashville, Tennessee. In 1968, he moved to Kinston, North Carolina, where in that same year he graduated from Granger High School.

The author received his Bachelor of Science Degree in Aerospace Engineering from North Carolina State University in 1972. Upon the completion of his active duty requirement in the North Carolina Army National Guard, he entered graduate school in 1973.

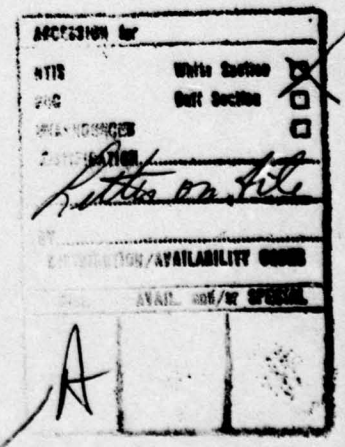

ACKNOWLEDGMENTS

The author would like to express his appreciation to Dr. F. R. DeJarnette for his guidance and direction, and to Mr. J. J. Murray, U. S. Army Research Office, for his guidance and conception of this investigation. This research was supported under Grant No. DAHC04-74-G-0007 and Grant No. DAHC04-75-C-0023 with the U. S. Army Research Office, Research Triangle Park, North Carolina.

TABLE OF CONTENTS

LIST OF FIGURES

LIST OF SYMBOLS

AR	aspect ratio, b^2/S_o
b	wing model span, inch
c	wing model chord, inch
C_D	drag coefficient, D/qS
C_L	lift coefficient, L/qS
$C_{L_{max}}$	maximum lift coefficient
C_{D_T}	total drag coefficient, D_T/qS
C_{L_T}	total lift coefficient, L_T/qS
C_p	pressure coefficient, $(p - p_\infty)/q$
d	proprotor diameter, feet
D	wing drag or drag component of proprotor axial force, pounds
D_T	total drag, wing drag combined with drag component of proprotor axial force, pounds
h	proprotor height, inch
J	advance ratio as designated for propellers, V/nd
L	lift, wing lift or lift component of proprotor axial force, pounds
L_T	total lift, wing lift combined with lift component of proprotor axial force, pounds
n	proprotor shaft speed, Ω/60, revolution per sec (rps)
p	static pressure, lb/ft^2
p_∞	free stream pressure, lb/ft^2
q	free stream dynamic pressure, $1/2\ \rho\ V^2$, lb/ft^2
RP	proprotor pitch, degrees

RL	proprotor horizontal location with respect to the wing model, fraction of chord measured from the wing leading edge.
S	wing planform area, ft^2
S_o	wing planform area, in^2
t_{max}	wing maximum thickness, inch
T	proprotor axial force, pounds
T_∞	free stream temperature, °F
V	free stream velocity, ft/sec
x	horizontal distance from wing leading edge, inch
y	vertical distance above wing, inch
α	wing model angle of attack, degrees
ΔC_L	change in lift coefficient
λ	proprotor shaft tilt angle from vertical; positive angles designate angle in which proprotor shaft is tilted forward of the hub in the test section (See Fig. 19)
ρ	free stream density, $slug/ft^3$
Ω	proprotor shaft speed, rpm

SUMMARY

An experimental investigation was conducted in the North Carolina State University subsonic wind tunnel to determine the interference effects of a proprotor and a wing on their lift and drag characteristics. It was theorized that the oncoming stream would sweep the wake of the proprotor over the top of the wing resulting in favorable interference effects, i.e. an increase in the lift and decrease in the drag. To test this theory, a wing was mounted in a cantilever fashion in the test section of the wind tunnel and a proprotor was positioned above the wing on a shaft through the ceiling of the test section. Lift and drag forces were measured on the wing and axial loads on the proprotor for test section velocities from 0 to 60 ft/sec and proprotor shaft speeds from 0 to 500 rpm. Test conditions varied the wing angle of attack and proprotor tilt angle, position, and shaft speed. Five different wing models were used and one was constructed to measure the pressure distribution.

The results showed significant increases in lift and decreases in drag for both the wing and proprotor as a result of favorable interference near the stall angle of attack of the wing. Below the stall, favorable interference effects were small. More favorable results were obtained for the proprotor shaft tilted forward to about 10°, while unfavorable results were found for a tilt angle of 22.8° and negative tilt angles. The proprotor shaft speed and height above the wing had a significant effect on the results while the chordwise position was insignificant.

The results show that the favorable interference effects of this arrangement makes it attractive for V/STOL and helicopter operations.

INTRODUCTION

Advances in short take-off and landing (STOL) and vertical take-off and landing (VTOL) aircraft have been extensive in the past two decades. These technology advances have led to corresponding increases in aircraft mechanism complexity, maintenance, and operation costs. In addition, they have diverted some of the interest in the area of V/STOL aircraft to proprotor aircraft, commonly called convertiplanes. Convertiplanes have been on designers drawing boards since the early 1950's, and several have been built and tested. Convertiplanes, for the most part, involve two basic design concepts. One concept uses a semi-rigid proprotor which operates with cyclic pitch like a helicopter in the hover mode and as a propeller in horizontal flight. This concept is illustrated by the Bell XV-15 shown in Figure 1. The other convertiplane concept involves a tilting propeller-wing assembly, such as the design used on the Vertol Model 76 Tilt-Wing Convertiplane.

Paralleling these convertiplane designs, research in the area of V/STOL aircraft has been directed primarily toward the improvement of basic tilt-rotor aircraft technology. Detore and Sambell (ref. 1), in their study of 1985 commercial tilt-rotor transports, looked at tilt-rotor noise levels as well as more general aspects of convertiplane performance. Additional research has been devoted to the exploration of the aerodynamics of wing and proprotor configurations. Huffman and Jackson (ref. 2) studied static wing lift capabilities in a powered ground effect mode. Makofski and Menkich (ref. 3) considered air loads on flat panels in a rotor slip stream, and Draper and Kuhn (ref. 4) studied the aerodynamics of a wing and propeller combination.

Although research on V/STOL aircraft has been extensive, there are other convertiplane configurations yet to be studied. One such configuration, somewhat like the Bell XV-15, has counter rotating proprotors, with horizontal tilting capabilities, located at each wing tip, but the wings also have rotational capabilities. The important concept which distinguishes this design from the Bell XV-15 is that the propeller-rotor, hereafter designated as a proprotor, does not have the cyclic pitch mechanism required by the XV-15 for hover operation. This new concept involving a proprotor which operates solely as a propeller was conceived by J. J. Murray, Director, Engineering Sciences Division, U. S. Army Research Office. He theorized that a proprotor operating over a wing in forward flight would cause an additional velocity increment on the wing's upper surface due to the wake of the proprotor being swept down stream by the on-coming stream velocity (See Fig. 2). This additional upper surface velocity, caused by favorable proprotor interference, would reduce the upper surface pressure, increase the lift, delay boundary-layer separation and decrease the wing drag. It was also theorized that the wing might provide favorable interference effects on the proprotor. A proprotor operating near the wing's upper surface may experience a "ground effect" that would increase the lift of the proprotor. The combination of additional wing lift and reduced drag, plus the improved lift properties of the proprotor would make this concept attractive for future design considerations.

Previous investigations of tilting proprotor concepts have considered the overall aerodynamic characteristics of specific designs. It is the purpose of this research to experimentally investigate the lift and drag characteristics of a constant-pitch proprotor and wing interaction system in the North Carolina State University subsonic wind tunnel.

Next page

DESCRIPTION OF APPARATUS

The testing system consisted of five basic parts, the proprotor and wing models, the North Carolina State University subsonic wind tunnel, the strain gage balance system, the system instrumentation, and the proprotor alignment, drive and shaft assembly. The overall system is illustrated in Figure 3, 4, and 5. Figure 3 illustrates the North Carolina State subsonic wind tunnel facility. The basic wing and proprotor testing configuration is represented in Figure 4. Figure 5 is an overall system view of the wind tunnel which indicates the proprotor alignment, drive, and shaft assembly above the wind tunnel.

Proprotor and Wing Models

Proprotor

A two-blade proprotor, 39-5/16 inches in diameter, with a machined aluminum leading edge and balsa trailing edge was used for the tests (See Fig. 6). The proprotor blades each have 1.475 inch chord with an NACA 23112 airfoil section. The proprotor had a 1/2 inch long cylindrical aluminum hub, 1-15/16 inches in diameter, as shown in Figure 6. This figure also illustrates the threaded rods and locking nuts used to secure the blade to the proprotor hub. This method of securement allows for variation in blade pitch. A blade pitch of 10° was used in all interference testing. This value was determined from tests run to determine proprotor axial force as a function of blade pitch.

Additional proprotor testing involving the test section wall interference was also performed. Information involving this testing is described in the section on system calibration.

Wing Models

Five wing models were tested in this investigation. The models consisted of wings with airfoil sections of a flat plate, N29, NACA 4415, Bensen G-2, and NACA 2415. The wing models used in the force measurement investigations, which include all but the NACA 2415 wing model, are illustrated in Figures 7 and 8. The remaining NACA 2415 wing model (See Fig. 9) was employed in the pressure distribution testing. A description of the models can be found in Table 1 on the following page.

TABLE 1. Wing Models Description

Flat Plate Model

Chord	:	4 inches
Span	:	22 inches
Thickness (Max)	:	.25 inches
Balance Securement Location	:	c/4
Aspect Ratio	:	5.5
Area	:	.6111 ft^2
Machined Round Leading and Trailing Edges		
Material	:	Aluminum

N29 Wing Model

Chord	:	5 inches
Span	:	22 inches
Thickness (Max)	:	1.125 inches
Balance Securement Location	:	c/4
Aspect Ratio	:	4.4005
Area	:	.76388 ft^2
This Model Had a Drag Fairing on the Balance Mount for Drag Reduction (See Fig. 10)		
Fairing Airfoil Section	:	NACA 2431

NACA 4415 Wing Model

Chord	:	6 inches
Span	:	22 inches
Thickness (Max)	:	.72 inches
Balance Securement Location	:	c/4
Aspect Ratio	:	3.666
Area	:	.91666 ft^2
Material	:	Wood

Bensen G-2 Wing Model

Chord	:	6.375 inches
Span	:	22 inches
Thickness (Max)	:	.71875 inch
Balance Securement Location	:	3/4
Aspect Ratio	:	3.451
Area	:	.97395 ft^2

This Model is a Section Taken From a Bensen Gyrocopter Blade

Material : Wood with Steel Reinforcement

NACA 2415 Wing Model

Chord	:	10.5 inches
Span	:	26 inches
Thickness (Max)	:	1.5 inches
Aspect Ratio	:	2.4762
Area	:	1.8958 ft^2

This Model was of a Rib Construction with 23 Pressure Tabs Distributed Over the Upper and Lower Surfaces 10-3/4 inches from the wing root

Pressure Tab x/c Locations are as Follows:

Upper Surface		Lower Surface	
Tap No.	x/c	Tap No.	x/c
1	0	14	.015
2	.005	15	.035
3	.015	16	.06
4	.035	17	.098
5	.055	18	.148
6	.095	19	.232
7	.145	20	.358
8	.195	21	.512
9	.275	22	.682
10	.395	23	.879
11	.525		
12	.695		
13	.865		

North Carolina State University Subsonic Wind Tunnel

The wind tunnel facility at North Carolina State University is a Merrill subsonic wind tunnel capable of test section speeds in the range from zero to approximately 100 miles per hour (See Fig. 5). The tunnel is of the continuous flow, single return type with a vented test section. The test section is 45 inches wide, 32 inches high, and 46 inches long. The wind tunnel side walls in the test section provide model observation through large plexiglass windows. The wind tunnel is powered by a 50 horsepower constant speed induction motor which drives a three bladed variable pitch fan. The air speed in the tunnel is controlled by varying the pitch of the fan blades. Figure 5 represents the wind lab facility. The tunnel employes two 10 mesh screens located upstream of the test section to reduce the turbulence in the test section. The flow conditions in the test section maintain a turbulence factor of 1.26 at a velocity of 60 mph. The nonuniformity in the test section is less than 2%.

Wing and Proprotor Force Balance System

Wing Force Balance

A force balance system involving the use of foil type electrical strain gages was used to measure the wing lift and drag forces and also the proprotor axial forces. The force balance for the measurement of wing model loads was constructed from a 13 inch length of 1.0 inch square 2024-T4 Aluminum stock. This balance made use of four machined cross sections equipped with strain gages, two for the lift component, and two for the drag component of the force measured (See Fig. 11). The cross section machined for the larger lift components had a thickness 0.488 ± .022 inches. A smaller more sensitive drag component cross section was machined

to a thickness of .183 ± .022 inches. The use of a four arm strain gage bridge circuit in this balance allowed for temperature compensation between gages and for different force span locations for different wing models used. Strain gages used in the bridge circuit for each component were 120.0 ± .15% ohm micromeasurement gages. The gage factor for each gage was indicated by micromeasurement gages as 2.09 ± .5%.

Proprotor Axial Load Strain Gage Balance

The proprotor axial load force balance was constructed from a four inch length of 1/8 inch by 7/8 inch 2024-T4 Aluminum stock. A two arm temperature compensating strain gage bridge circuit incorporating two 120.0 ± 15% ohm micromeasurement strain gages was used. A four arm bridge necessary for compensation of varying location of load application was not required because the proprotor axial force point of application was the same in each test. The balance system was designed using a relatively thick 1/8 inch cross section and a bearing pivot arrangement at the point of load application (See Fig. 12). This design allowed only small proprotor axial deflections which provided a constant test configuration. The bearing pivot arrangement allows the proprotor shaft to transmit the axial force to the balance while rotating and ensures that even with deflection the load will be applied perpendicularly to the balance beam. The balance alignment with the proprotor shaft was a critical part of the force balance-proprotor shaft arrangement. Figure 13 exhibits the alignment system used. This figure shows a rigid square, steel, channel mount support which allows the balance beam to obtain the alignment angle necessary for the tilted proprotor tests. The actual balance mounting, displayed in Figure 14, makes use of alignment screws to ensure perpendicular alignment with the proprotor shaft.

System Instrumentation

Force Balance Instrumentation

A Vishay/Ellis-20 Digital Strain Gage Indicator was used in the measurement of wing model lift and drag loads and proprotor axial loads (See Fig. 15). This instrument was designed primarily for use with resistive type strain gages or strain-gage devices to determine numerically the strain in a structure. The instrument has quarter, half and full bridge capabilities. The half or two arm bridge was used to determine the proprotor axial loads. A full or four arm bridge was used in lift and drag measurements on the wing models. This instrument employed a feature which allowed the selection, in discrete steps, of the current through the strain gage balance input bridge. This feature, the Span Coarse selector, allowed a variation of the strain gage excitation voltage and thus, the numerical readout of the instrument for known balance loads. This capability was very useful in the calibration of the strain gage force balance system (See System Calibration).

Test Parameter Instrumentation

Three investigation test variables used in each test series needed to be monitored, the test section velocity, V, the proprotor speed, Ω, and the wing model angle of attach, α. The test section velocity was maintained at the desired value by using a Merrill inclined manometer supplied with the wind tunnel facility. A more sensitive manometer was constructed as a backup check and can be seen in Figure 5. The wing model angle of attack was measured using a bubble level which was accurate to within $\pm$ 1/2°. The proprotor speed, Ω, was measured using a Strobotac.

In the wing lift and drag investigation, a number of pressure distribution tests were performed which required a pressure measurement instrument. These tests employed an inclined multiple bank manometer shown in Figure 16. This instrument was manufactured by T. E. M. Instruments Ltd.. It has a 36 bank capability with a maximum 25 inch possible fluid displacement. The instrument is inclinable up to 90°. A specific gravity fluid of .827 was used in all pressure tests. The instrument was graduated in tenths of one inch and using a manometer inclination of 30° readings accurate to the nearest .05 inch were obtainable.

Proprotor Alignment, Drive, and Shaft Assembly

Proprotor Shaft Assembly

The proprotor shaft assembly must transmit torque to the proprotor hub and convert any axial proprotor loading into a linear displacement for measurement. The shaft consists of an outer torque transmitting hollow shaft, an inner solid rod on which the proprotor hub is mounted, and a system of bearings which allow axial inner shaft displacement while transmitting torque to the proprotor hub (See Fig. 17).

The outer shaft, a 24 inch length of thick walled pipe, was machined to two different diameters. A 5/8 inch diameter corresponding to the pillar block bearings that was used in the shaft bearing housing (See Description Bearing Housing). The test section end of the shaft was machined to a larger 11/16 inch diameter to provide additional shaft rigidity. The inner shaft was a 27-3/4 inch length of 5/16 inch polished steel with a 5/8 inch piece of steel fixed to the end to accommodate the proprotor hub. Teflon bushings pressed into the ends of the hollow outer shaft provided sliding movement of the inner shaft within the outer shaft

(See Fig. 17). Torque transmission to the inner shaft was accomplished by supplying a moment from the outer shaft to ball bearings pressed in the inner shaft. The ball bearings were restricted to a machined 1/4 inch slot in the outer shaft while secured to an 1/8 inch rod pressed into the inner shaft. Using this system, a torque could be supplied to the bearings and thus, the inner shaft while rotating was free to move in the axial direction perpendicular to the torque.

Proprotor Shaft Bearing Housing Assembly

The bearing housing was a basic box construction which had two functions. This structure had to supply a rigid movable base capable of aligning the proprotor for each test case and house the bearings needed to provide a smooth rotational movement for the proprotor shaft. The housing was constructed of 3/4 inch plywood (See Fig. 18). Steel reinforcement on the housing base provided rigidity and acted as runners in the guider constructed on the outside of the wind tunnel ceiling. The guide runner arrangement and locking screws provided on the runners allowed a 2 foot variation in horizontal proprotor location with respect to the wing model in the wind tunnel test section (See Fig. 18).

Two self-aligning pillar block bearings were used in the housing assembly. A stationary lower bearing was used in a pivot fashion while a movable upper bearing was capable of changing position with respect to the lower pivot bearing by sliding along a slot in the housing construction. By moving the upper bearing along the slot and then securing it with bolts and a machined locking brace, the proprotor shaft was capable of obtaining an angle tilted from the vertical in the range from positive 22.8° to negative 10° (See Fig. 15). For a definition of proprotor size convention,

see symbol list. The major limitation in obtaining tilt angles was the proprotor blade length at the higher positive tilt angles where the blade tips approached the test section ceiling (See Fig. 19).

Proprotor Motor Drive

A Sears 1/4 hp variable speed motor was used to drive the proprotor by using a 5 to 1 belt-pulley arrangement (See Fig. 18). The motor was mounted in a housing constructed of 3/4 inch plywood. The front and rear of the motor housing are braced with a steel reinforcement which acts as a runner in the guides constructed on the outside of the wind tunnel ceiling (See Fig. 18). This arrangement provides a means by which the system can be moved horizontally. These reinforcements also provide locking screws to secure the motor mounting assembly when the test configuration has been obtained. An aluminum packing plate with machined arc guides provides a secure place to mount the motor to the housing. By using a pivot bolt and locking nut in conjunction with the machined backing plate arc guides, the motor can be tilted to the angle necessary to align the drive pulleys. The variable speed motor capabilities and the 1 to 5 drive arrangement allows proprotor speeds of 140 rpm to approximately 800 rpm.

SYSTEM CALIBRATION

Two different systems involving strain-gage force balances were employed in this investigation for measurement of aerodynamic loads. Wing lift and drag forces were measured by the strain-gage balance attached to the wing through the side wall of the test section (See Fig. 11). The calibration of the wing force balance was performed statically by direct application of known loads to the wing.

The measurement of the proprotor axial loads involved loads on a rotating shaft and thus required a more complex force measurement system (See description of Proprotor Shaft Assembly and Proprotor Force Balance Assembly). This arrangement depended on the linear displacement of the proprotor shaft due to proprotor axial air loads. It was found that the vibrations and bearing friction associated with the shaft rotation caused a static calibration of this force measurement system to be inaccurate. Therefore, a dynamic calibration procedure was developed whereby known loads were applied to the proprotor strain-gage balance system while the shaft assembly was rotating, but with the proprotor removed. The calibration loads were applied to the force balance in the positive (upward) direction by means of an overhead pulley system shown in Figure 20. The zero load point was made to account for the weight of the proprotor by applying a weight equal to the proprotor weight in the negative direction. This procedure allowed the system to rotate in a zero load configuration providing a situation in which known loads could be applied. Weights from 0 lbs. to 5 lbs. were used in the calibration, which is well within the range of the loads produced by the proprotor. A proprotor speed of 400 rpm was used for the calibration and the system was calibrated before each test.

TESTING PROCEDURE

The test program for the proprotor and wing interaction involved testing in two phases. Phase I tests determined the interaction effects of the proprotor on the wing lift and drag. Phase II was concerned with the effect of the wing interaction on the lift of the proprotor. Phase I tests included investigations of five different wing models having the following airfoil sections: a flat plate, NACA 4415, N29, Bensen G-2, and a NACA 2415. The lift and drag as a function of angle of attack was obtained for each wing first without interference effects by testing without the proprotor. The wing models were tested through an angle of attack range from 0° to 22° at a test section velocity of 43 ft/sec (a dynamic pressure of 2.02 lb/ft^2). This speed was used because it produced the desired advanced ratios for the later tests with the proprotor.

Interference effects of the proprotor on each wing were obtained by measuring the wing loads with the proprotor operating above the wing. Interference tests on all wing models except the N29 wing were basic investigations with the proprotor shaft in the vertical position. The interference tests on the N29 wing model were much more involved. These tests varied the proprotor speed, position, and inclination. The proprotor shaft speed was varied from 0 rpm to 400 rpm. The position of the proprotor was varied from 2 cm to 13 cm vertically above the wing and chord wise from the wing leading edge to the trailing edge. The tilt angles of the proprotor shaft were varied from + 22.8° to - 10.0° from vertical. In these tests the proprotor tilt angles are designated as positive when the proprotor shaft is upstream of the proprotor in the test section (See Fig. 19). The combination of wind tunnel speeds and proprotor shaft speeds

represents a variation in proprotor advance ratio, J, from 1.079 to 2.749. The advance ratio, J = V/nd, is the parameter used in propeller terminology. The proprotor blade pitch was maintained at 10° throughout the entire investigation. This blade pitch value, 10°, was determined to be the blade pitch angle which produced the largest proprotor lift loads.

A preliminary investigation of test conditions at a speed of 43 ft/sec and proprotor shaft speed of 400 rpm verified that the interference from the wind tunnel walls and floor were insignificant. Calculations of the wind tunnel wall interference on rotors (ref. 13) indicated that only one parameter in this investigation would be affected, the proprotor blade pitch. Results of the calculations indicated that the maximum wall interference on the proprotor blade pitch, θ, would result in a 1.5° difference in the measured reading. Tests indicated that small changes in blade pitch were insignificant. The interference of the wind tunnel floor on the proprotor operation was also researched (ref. 14). If the floor should interfere with the proprotor wake, then a vortex would travel along the floor upstream of the location of the proprotor*. This vortex can be detected by observing yarn tuffs placed along the centerline of the floor. If these tuffs point upstream, then a vortex is present and the floor interference is significant. Wind tunnel tests were performed with the tuffs attached to the floor, and no evidence of floor interference was detected.

The effects of the proprotor on the wing lift and drag were also explored by measuring the pressure distribution on the NACA 2415 wing model. The pressure distribution was measured as the wing angle of attack was varied from 0° to 20° in 5° increments. The test section velocity, as in

*Private communication with William H. Rae., Jr., Ph.D., University of Washington, Seattle, Washington, 1973.

the previous tests, was maintained at 43 ft/sec. The proprotor shaft was maintained in a vertical orientation 3 cm above the wing model quarter chord location at a speed of 400 rpm.

Phase II testing measured the interference effects of the N29 wing on the proprotor axial loads. Testing in this phase followed closely the procedure outlined in Phase I. Testing involved investigations of proprotor axial loads with and without wing interference.

RESULTS AND DISCUSSION

NACA 4415 and Bensen G-2 Wing Investigation

The NACA 4415 and Bensen G-2 wing models were tested with and without the proprotor to determine the interference effects. In the interference tests, the proprotor shaft was maintained vertical at the wing quarter chord position. Results from these tests indicate significant increases in the lift and decreases in the drag near the stall while only minor proprotor effects were detected at angles of attack below the stall. Graphical results of these tests are presented in Figures 21, 22, and 23.

Figure 21 shows the lift coefficient as a function of the angle of attack for the two wing models. The proprotor interference effects on the Bensen G-2 wing model increased the lift higher than any other model tested. The basic Bensen G-2 wing alone produced a $C_{L_{max}} = 1.10$ at a stall angle of attack of $\alpha = 14°$. The interference tests on this same model increased the stall angle by 6° and the wing lift coefficient to $C_L = 1.422$. This value is an 83% increase in lift coefficient over the value of the noninterference lift coefficient determined at the same wing angle of attack. Interference effects at angles of attack below stall increased the lift coefficient by a nearly constant value of 0.06.

The NACA 4415 wing model investigation also indicated significant lift improvements due to proprotor interference (See Fig. 21). Noninterference test data indicated $C_{L_{max}} = 1.24$ at $\alpha = 16°$. Interference testing at $\Omega = 400$ rpm resulted in a 2° delay in stall and a more gentle stall which is displayed over a 4° angle of attack range. Interference effects increased the maximum lift coefficient to 1.36. This value represents a 46.6% increase in the basic wing lift coefficient at $\alpha = 18°$. Interference

lift coefficients were about 0.08 higher than those of the basic wing below the stall.

Drag data resulting from proprotor-wing testing for the NACA 4415 and the Bensen G-2 wing models are illustrated in Figures 22 and 23. The decreases in drag displayed in these figures parallel interference lift improvements. Small drag changes were noted below the stall while significant decreases in drag were found in the stall region.

The NACA 4415 wing model tests showed that the proprotor interference caused a slight increase in drag below the stall. At wing angles of attack between α = 16° and α = 21.0° an interference drag reduction was noted (See Fig. 22). The maximum reduction in wing drag, a 27.9% decrease, was noted at α = 18°.

The drag characteristics of the Bensen G-2 model, as shown in Figure 23, indicate that the proprotor produced a more favorable interference effect than in the NACA 4415 wing test. The drag coefficient was decreased by a relatively constant value of .005 in the angle of attack range from α = 0° to α = 12°. A larger, more significant drag reduction was detected in the range α = 13° to α = 21°. A maximum 39.6% decrease in drag was realized at α = 18°. In both model tests, interference effects at large angles of attack (α > 21.0°) indicated the proprotor increased the wing drag.

N29 Wing Model Interference Effects

Vertical Proprotor Tests

Interference tests on the N29 wing model were conducted first with the proprotor shaft vertical and 3.0 cm above the wing quarter chord position. The proprotor speed was maintained at Ω = 400 rpm. Initial testing

concentrated on wing lift characteristics, and the results of these tests are presented in Figure 24. The proprotor interference resulted in a maximum lift coefficient $C_{L_{max}} = 1.495$ at $\alpha = 20°$. This value is a 2.99% increase in maximum lift coefficient over the noninterference value. A comparison of interference and noninterference lift characteristics indicate a more gentle stall in the interference case. The nearly flat stall region for the interference lift data resulted in a 2° delay in stall. The stall delay created a 64.8% increase in lift over noninterference data. In this same test, a relatively constant .03 increase in lift coefficient was realized below the stall.

Additional proprotor interference testing involved N29 wing drag measurements and the resulting data is presented in Figure 25. The data obtained from these tests can be generalized as a downward shift in the drag coefficient curve. A representative .01 decrease in drag coefficient was realized at low wing model angles of attack. The more gentle stall characteristics associated with the interference lift data is also indicated in the drag data. Gentle stall characteristics and a downward shift in drag coefficient resulted in a 29% decrease in drag coefficient at stall, $\alpha = 20°$. At zero angle of attack, the proprotor interference produced an 18% decrease in minimum drag coefficient. A 2° stall delay is indicated in the interference data compared with noninterference data.

Additional N29 wing tests resulted in information on the effects of proprotor speed and location on wing lift and drag characteristics. These tests were performed at $\alpha = 20°$ with the proprotor maintained vertical at a speed of $\Omega = 400$ rpm. The variation of proprotor location involved the height position above the wing and location along the wing chord.

Figure 26 is a graphical representation of the lift coefficient as a function of the test variables discussed above. The variation in proprotor chord location at a height of 3.0 cm resulted in wing lift coefficients that differed by less than 2%. Lift measurements in this test case were made at two wing angles of attack, $\alpha = 20°$ and $\alpha = 22°$. Higher lift coefficients were obtained at $\alpha = 20°$. This result is an indication that the proprotor, at smaller stall angles, is more effective in delaying boundary layer separation. Vertical hub height effects on proprotor lift coefficients are also presented in Figure 26. Data in this test was obtained with the proprotor located at the c/4 wing position. The lift data indicated a significant dependence on proprotor height. The maximum lift coefficient, $C_{L_{max}} = 1.45$ was obtained at the lowest proprotor height, 2.0 cm. With increase in proprotor height, the wing lift coefficient decreased to a value approaching the basic wing value, $C_L = .9$, at h = 13 cm. The interference effect of the proprotor on the wing lift was negligible for proprotor heights above 13 cm ($y/c \geq 1.0$). The final data curve presented in Figure 26 shows that the proprotor speed has a significant effect on the wing lift. Lift coefficients increased proportionally with increase in proprotor speed. A significant lift increase, associated with delay in boundary layer separation, was detected at a speed of $\Omega = 400$ rpm. Little effect of proprotor speed on lift coefficient was detected above $\Omega = 500$ rpm for this test section velocity, V = 43 ft/sec.

The interference effects of the proprotor on the wing drag were also determined and the data is presented in Figure 27. Drag measurements as a function of proprotor chord location indicated results similar to lift data. The wing drag was affected very little due to moving the proprotor location along the chord. The drag coefficient, as in the lift coefficient

case, had a significant dependence on proprotor height and speed. In tests where the proprotor height was varied, the drag was reduced as the proprotor was raised to a position about y/c = 0.5. For proprotor heights above y/c = 0.5, the proprotor down-wash was unable to delay boundary layer separation and the drag increased 37.1%. Tests in which the proprotor shaft speed was varied also indicated the delay in boundary layer separation. Very little effect on drag is detectable for changes in the proprotor speed for speeds below Ω = 300 rpm. However, at a proprotor speed of Ω = 300 rpm, the drag is reduced 48.5%. Further increases in proprotor speed resulted in only a 4% increase in drag.

Tilted Proprotor Tests

Interference tests where the proprotor shaft was tilted were performed in a fashion similar to the noninterference tests performed on the N29 wing model. These tests involved proprotor tilt angles in the plane perpendicular to the wing axis pivoting about the upper wing surface c/4 position. For a definition of proprotor tilt angle sign convention see the List of Symbols. Results of this investigation involved interference wing lift and drag characteristics (See Figs. 28 and 29).

Larger increases in $C_{L_{max}}$ and lift coefficients in the linear portion of the lift curve were noticed at small positive tilt angles. Negative tilt angles resulted in destructive lift interference.

At a proprotor tilt angle of λ = 22.8° the maximum interference wing lift coefficient was $C_{L_{max}}$ = 1.50. This value represents a 3.42% increase over the noninterference value. The interference effects in this test case produce a more linear lift curve at lower angles of attack. Interference lift data does not have the change in lift slope associated with

the noninterference data. A lift coefficient of C_L = 1.50 measured at α = 20°, represents a 2° delay in the wing stall and a 65% increase in lift over the noninterference values at the same angle of attack. Drag data measured in interference testing at λ = 22.8° resulted in a relatively constant .005 decrease in drag coefficient over the noninterference drag curve. As with lift, larger interference advantages were realized at stall. Drag tests at α = 20° resulted in a 36% decrease over noninterference data.

Interference tests made at λ = 10.8° resulted in the most desirable stall characteristics of all the tilt configurations tested. The λ = 10.8° test data exhibited the largest increase in lift coefficient at stall, 67.9%. The stall characteristics of this test configuration are displayed in Figure 28. The data indicates a gentle stall with only a 4.44% decrease in lift coefficient over a 4° stall range. Lift data in the linear portion of the lift curve exhibited a relatively constant 0.06 increase in lift coefficient.

Drag data measured for the λ = 10.8° test case also indicated favorable interference effects (See Fig. 29). A drag decrease of 30.7% was measured at a stall angle α = 20° as well as a measured drag decrease of 21.3% at α = 22°. The stall drag characteristics indicate a delay in drag increase and display no severe drag jump as indicated in the noninterference case. The drag advantages resulting from interference at low wing angles of attack vary. The largest drag decrease at small angles of attack, 18%, occurs at α = 0. As α is increased, the drag data approaches the noninterference data. Drag decreases at α = 10° and α = 18° are 10.3% and 1.3%, respectively.

NACA 2415 Pressure Distribution Investigation

Pressure distribution tests on the NACA 2415 wing utilized proprotor speeds of Ω = 400 rpm and a proprotor c/4 wing location. Effects of the proprotor interference were most pronounced at stall angles of attack (See Fig. 30). The noninterference data, $\alpha = 20°$, in Figure 30 is represented by the lower pressures on the wing upper surface and the higher pressures on the lower surface. These conditions are indicative of a separated boundary layer on the wing's upper surface. The interference data presented in Figure 30 exhibits a pressure distribution characteristic of wings at large angles of attack without boundary layer separation. There is an increase in velocity noted on the wing's leading edge as indicated by the large negative pressure coefficients associated with small x/c values. The pressure coefficients increase with decreasing upper surface velocity as values of x/c approach unity. Slower velocities on the wing's lower surfaces were indicated by the higher interference pressure coefficients in this region. The combination of increased upper surface velocity and decreased lower surface velocity creates a more favorable lift in the stall region due to interference effects.

The pressure distribution measured at lower wing angles of attack showed very little effect of proprotor interference. This result confirms the small interference effects noted in lift and drag tests below the stall angle.

Proprotor Axial Force Investigation

The results from a series of investigations concerning wing interference effects on the proprotor axial force are represented in Figures 31-36. This graphical data involves the following investigative areas:

proprotor axial force as a function of the proprotor tilt angle, λ, proprotor hub height, h, and proprotor advance ratio, J = V/nd.

Figure 31 presents noninterference vertical proprotor lift data as a function of advance ratio. As the figure displays, each change in proprotor shaft speed and thus advance ratio results in a data curve which is a member of a family of curves. As the proprotor speed, Ω, was increased from 400 rpm to 450 rpm and from 450 rpm to 500 rpm, the curves were shifted upward by ΔC_L = .335 and ΔC_L = .425, respectively.

Figure 32 presents the change in proprotor lift data as a result of varying the proprotor tilt angle. The lift coefficients in Figure 32 were calculated based on the lift component of the proprotor axial force. The radial proprotor loads were not measured in this investigation. Figure 32 indicates a larger proprotor axial force and hence a larger proprotor lift coefficient at negative proprotor tilt angles. The decreased axial forces measured at positive proprotor tilt angles resulted in smaller proprotor lift coefficients. In the positive proprotor tilt angle range, the proprotor axial force and thus lift coefficient decreased almost linearly with increased tilt angle.

Interference proprotor lift tests indicated improvements in proprotor lift characteristics at low tilt angles ($\lambda < 18°$). For the larger tilt angles, $\lambda = 22.8°$ and $\lambda = 18°$, the wing interference effects on the proprotor were unfavorable and indicated significant decreases in lift. Figures 33 and 34 present data resulting from proprotor interference tests for $\lambda = 0°$ and $\lambda = 10.8°$. The data in these figures show a relatively constant lift coefficient over the entire wing angle of attack range. The maximum deviation in lift coefficient was approximately 12%. In Figure 33, $\lambda = 0°$, the data shows that more favorable interference is realized at the

larger proprotor speeds. This result confirms previous vertical proprotor test data. Interference proprotor data obtained from $\lambda = 10.8°$ tests indicate larger increases in lift coefficients at lower proprotor speeds, $\Omega = 400$ rpm. Negative proprotor tilt angles resulted in unfavorable interference data. All values of interference proprotor loads for the negative tilt angle case were significantly lower than the noninterference loads.

Further tests involving proprotor interference lift loads indicated some dependence on the proprotor location. Figures 35 and 36 present data from N29 wing tests ($\alpha = 22°$) where proprotor lift was measured as a function of proprotor height and chord location. Figure 35 gives lift data as a function of chord location. Proprotor lift measurements were made as the proprotor hub was positioned at locations varying from the wing loading edge to the trailing edge. The test results indicate little change as the proprotor chord location was varied. Larger changes in lift were indicated at larger proprotor speeds ($\Omega = 500$ rpm) in this test. The maximum variation in proprotor lift coefficient was approximately 12%.

Figure 36 presents data from N29 wing tests ($\alpha = 22°$, RL = c/4) where proprotor lift was measured as a function of proprotor hub height. This figure illustrates a family of curves as the height was varied for each proprotor speed tested. For proprotor speeds above $\Omega = 400$ rpm, maximum lift coefficients occurred at a proprotor height of 5.0 cm. At all three proprotor speeds tested, a unfavorable interference caused low lift coefficients at 4.0 cm.

Combined Proprotor and Wing Lift and Drag

The combined proprotor and wing lift and drag are the summation of the individual lifts and drags of the wing and proprotor. The lift and drag coefficients of the proprotor as well as the wing are based on the planform area of the wing. The N29 wing is used in this investigation. The only force measured on the proprotor is the force in the direction of the proprotor shaft. Since the shaft may be tilted with respect to the velocity in the test section of the wind tunnel, this force has a component in the direction of the wing lift and a component in the direction of the wing drag. The combined lift and drag data are called total lift and drag, and they are presented in Figures 37 and 38 both with and without the interference effects. The combined lift and drag without interference effects are the sum of the lift and drag of the wing alone and the proprotor alone.

Figure 37 exhibits the total lift coefficient as a function of angle of attack for three of the positive proprotor tilt angles tested. The unfavorable interference of negative tilt angles reduce the total lift coefficients and increase the drag coefficients and are not indicated here. The largest advantage realized in the interference total lift coefficient over the noninterference value occurred at a proprotor tilt angle of 10.8°. A total lift increase of 38.3% was found at a system stall angle of α = 20°. Smaller overall lift increases over noninterference lift were indicated at a proprotor tilt angle of λ = 0°, but it is important to note that the largest overall total lift coefficients occurred in this test configuration. The largest measured total lift coefficient was C_{L_T} = 3.91 at λ = 0°, h = 3.0 cm, RL = c/4, Ω = 400 rpm, and α = 15°. As the proprotor tilt angle was increased to λ = 22.8°, the system interference effect

became less favorable as shown in Figure 37. At these larger proprotor tilt angles (λ = 18°, λ = 22.8°) the interference effects at low angles of attack are unfavorable, but favorable interference is indicated in the stall region. At a proprotor tilt angle of 22.8°, favorable interference increased the total lift 22.1% over the noninterference value at the stall angle of α = 20°.

The combined (total) proprotor and wing drag characteristics are presented in Figure 38. The noninterference data in this figure indicate lower total drag coefficients for larger proprotor tilt angles. This result is anticipated for noninterference data because of the thrust component of the proprotor axial force which exists for positive proprotor tilt angles. For larger tilt angles, larger thrust components exist which, when added to wing drag, cause lower total drag.

Interference data, on the other hand, indicates a slightly different total drag characteristic. Data indicates large drag coefficients for the vertical proprotor test case as in the noninterference case. But, because of the favorable interference for a proprotor tilt angle of λ = 10.8°, the interference total drag for this tilt angle is as low as the noninterference data for a tilt angle of λ = 22.8°. Except for the λ = 22.8° tilt angle, favorable interference was found to be large near the stall region, but small below the stall. The largest decreases in drag were noted for a proprotor tilt angle of λ = 10.8°, although a small increase in drag was noted near α = 20° which is near the beginning of stall. The λ = 22.8° case was found to be different from the other tilt angles because unfavorable interference was found, as shown in Figure 38.

CONCLUSIONS

From the results of this investigation, the following conclusions are drawn:

1. Significant increases in wing lift, decreases in wing drag and a delay in stall can be achieved through favorable proprotor interference.
2. Favorable interference effects are large in the stall region but small below the stall.
3. Favorable proprotor interference occurs at small proprotor tilt angles $\lambda \leq 10.8°$. A positive tilt angle of $\lambda = 22.8°$ and small negative angles ($0 \geq \lambda \geq -10°$) produce unfavorable interference.
4. Favorable proprotor interference is affected significantly by proprotor shaft speed and height, but only slightly by horizontal position (for the hub remaining within the region of the wing chord).
5. Favorable interference of the wing on the proprotor increases the proprotor lift.
6. Favorable wing interference on the proprotor is affected little by proprotor horizontal position (within the region of the wing chord), but significantly by proprotor height and shaft speed.
7. The favorable interference of both wing and proprotor results in a significant improvement in the lift and drag of the combination of the wing and proprotor.

LIST OF REFERENCES

1. Detore, J. A.; and Sambell, K. W.: Conceptual Design Study of 1985 Commercial Tilt Rotor Transports, Vol. I - VTOL Design Summary, NASA CR-2544, May 1975.

2. Huffman, J. K.; and Jackson, Jr., C. M.: Investigation of the Static Lift Capability of a Low-Aspect Ratio Wing Operating in a Powered Ground-Effect Mode, NASA TM X-3031, July 1974.

3. Makofski, R. A.; and Menkick, G. F.: Investigation of Vertical Drag and Periodic Airloads Acting on Flat Panels in a Rotor Slipstream, NACA TN 3900, Dec. 1956.

4. Draper, J. W.; and Kuhn, R. E.: Investigation of the Aerodynamic Characteristics of a Model Wing-Propeller Separately at Angles of Attack Up to 90°, NACA TN 3304, Nov. 1954.

5. Ganzer, V. M.; and Rae, Jr., W. H.: An Experimental Investigation of the Effect of Wind Tunnel Walls on the Aerodynamic Performance of a Helicopter Rotor, NASA TN D-415, May 1960.

6. Heyson, H. H.: Linearized Theory of Wind Tunnel Jet-Boundary Corrections and Ground Effect for VTOL-STOC Aircraft, NASA TR R-124, 1962.

7. Lichten, R. L.: Some Performance and Operating Characteristics of Convertiplanes, SAE Report No. 221, Sept. 1957.

8. Lichten, R. L.: Some Aspects of Convertible Aircraft Design, Journal of the Aeronautical Sciences, Vol. 16, No. 10, Oct. 1949.

9. Stuart, III, Joseph: Tilt Wing Propelloplane Design Requirements, Journal of the American Helicopter Society, Vol. 2, No. 2, April 1957.

10. Johnson, W.: Analytical Modeling Requirements for Tilting Proprotor Aircraft Dynamics, NASA TN D-8013, July 1975.

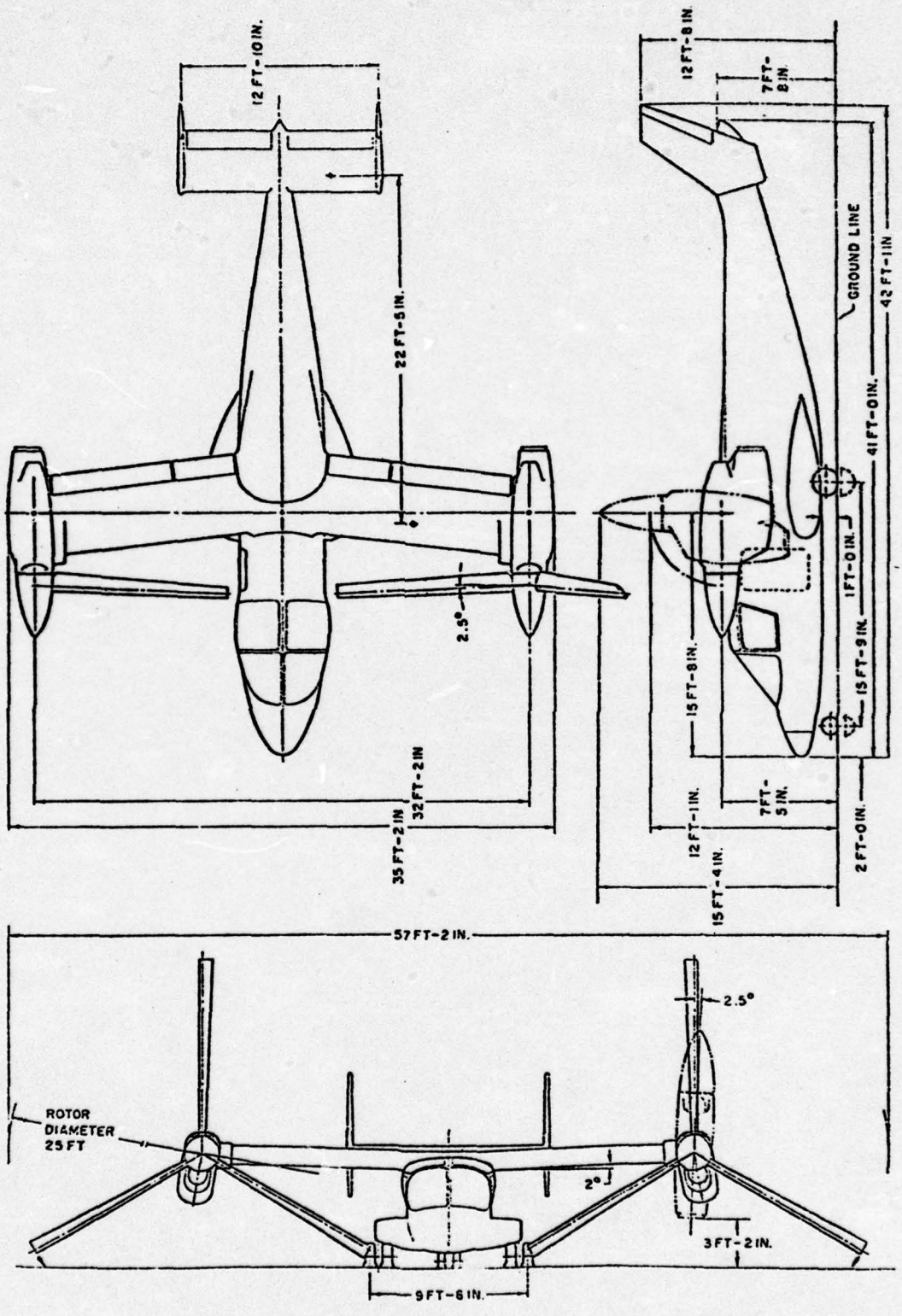

FIGURE 1. Bell XV-15

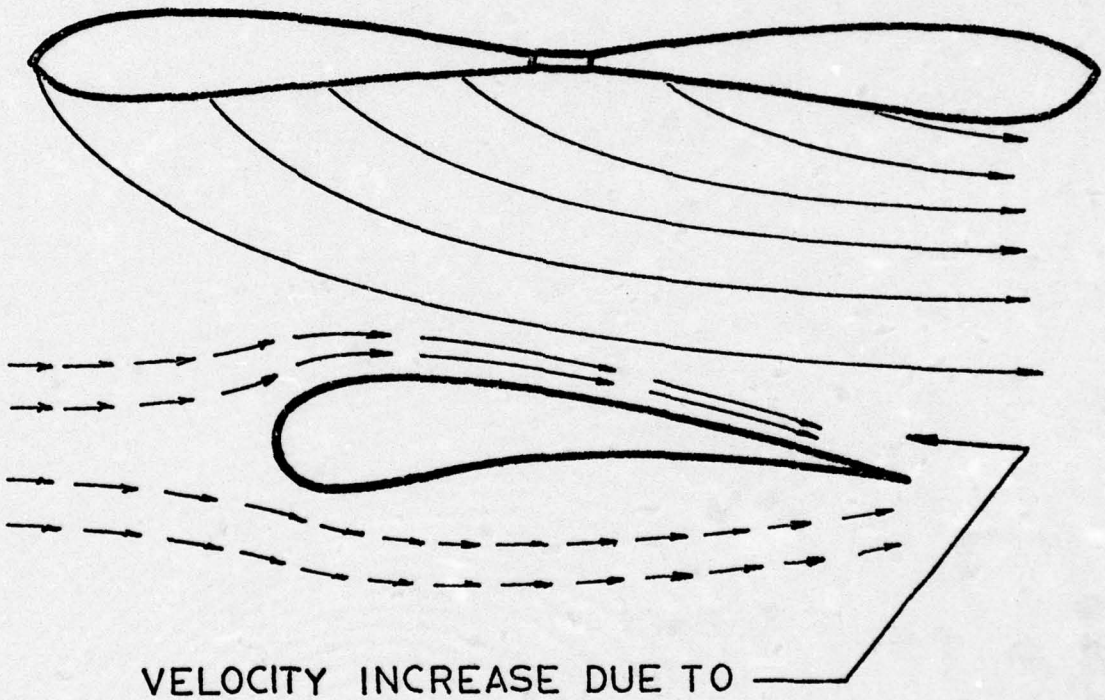

FIGURE 2 EFFECT OF PROPROTOR WAKE ON UPPER SURFACE VELOCITY

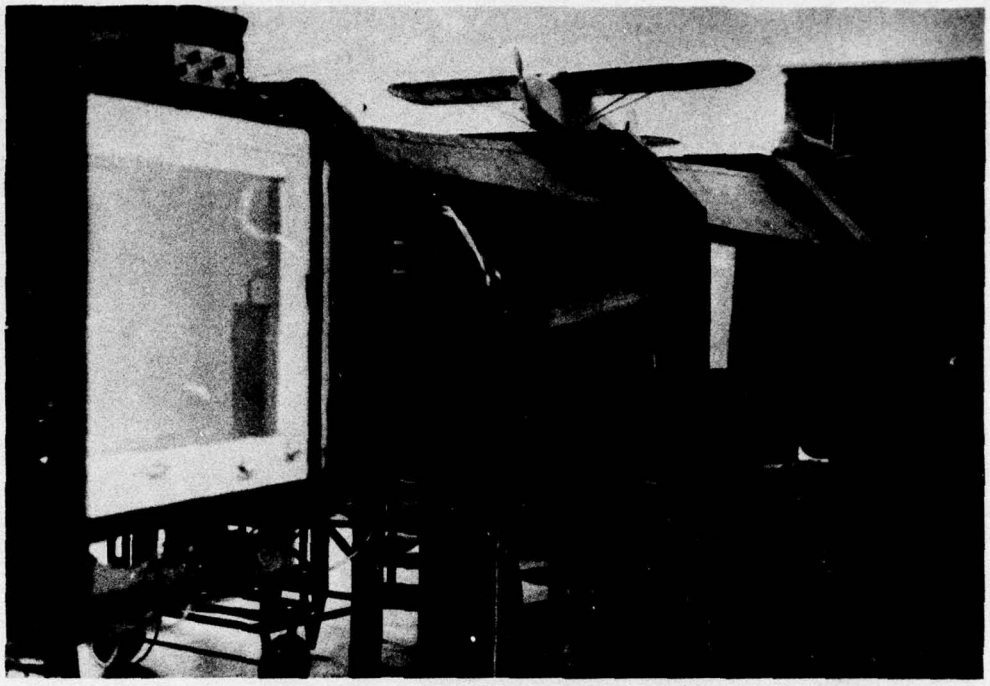

FIGURE 3. North Carolina State University Subsonic Wind Tunnel

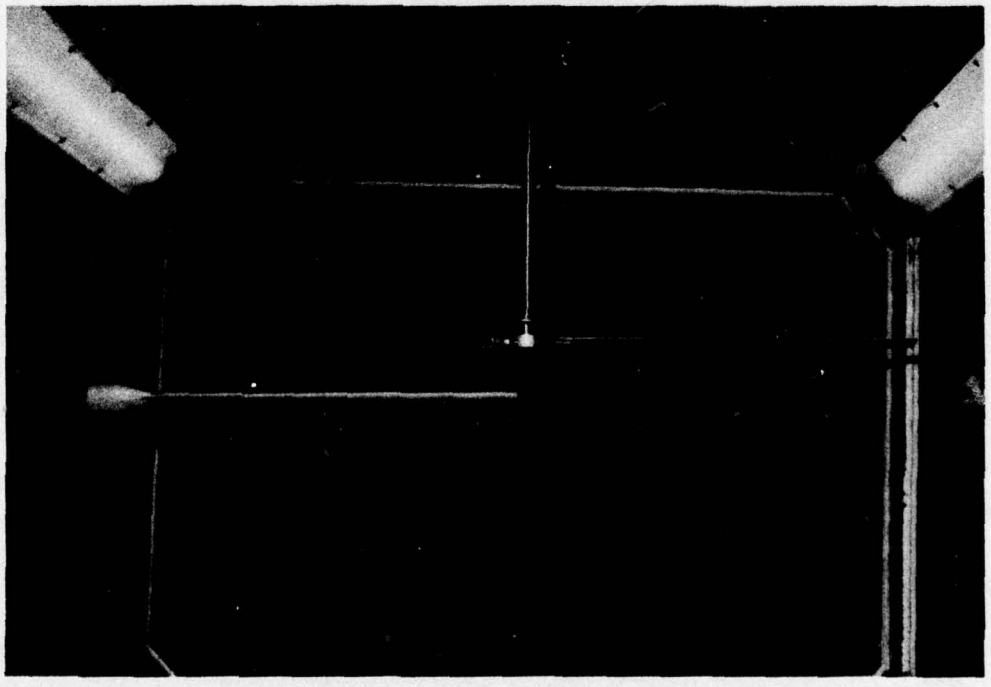

FIGURE 4. Down-Stream View of Wing and Proprotor in the Test Section

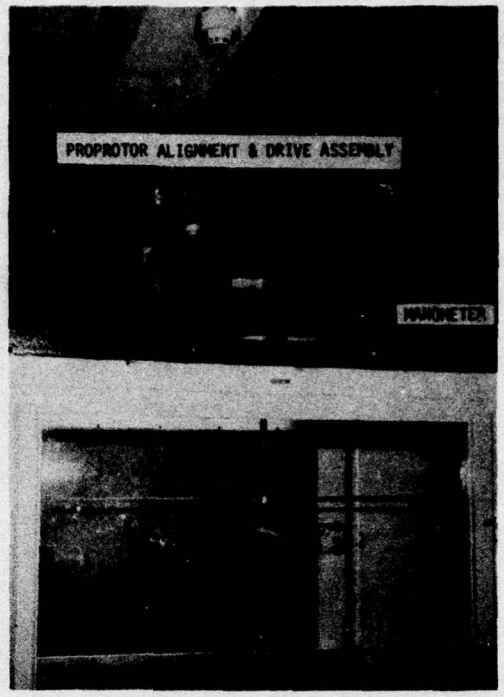

FIGURE 5. Side View of Overall Testing System

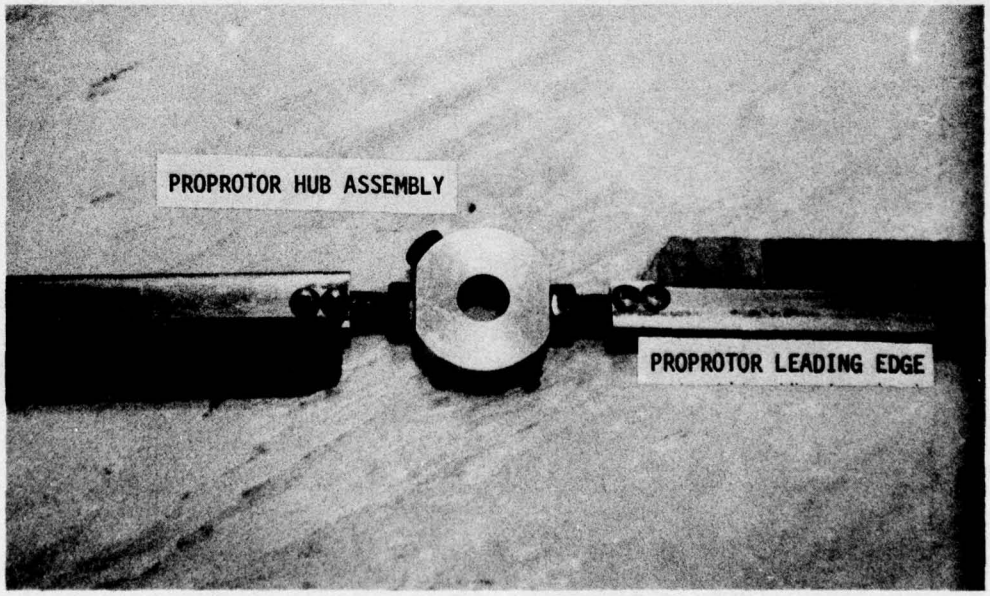

FIGURE 6. Proprotor Hub Assembly

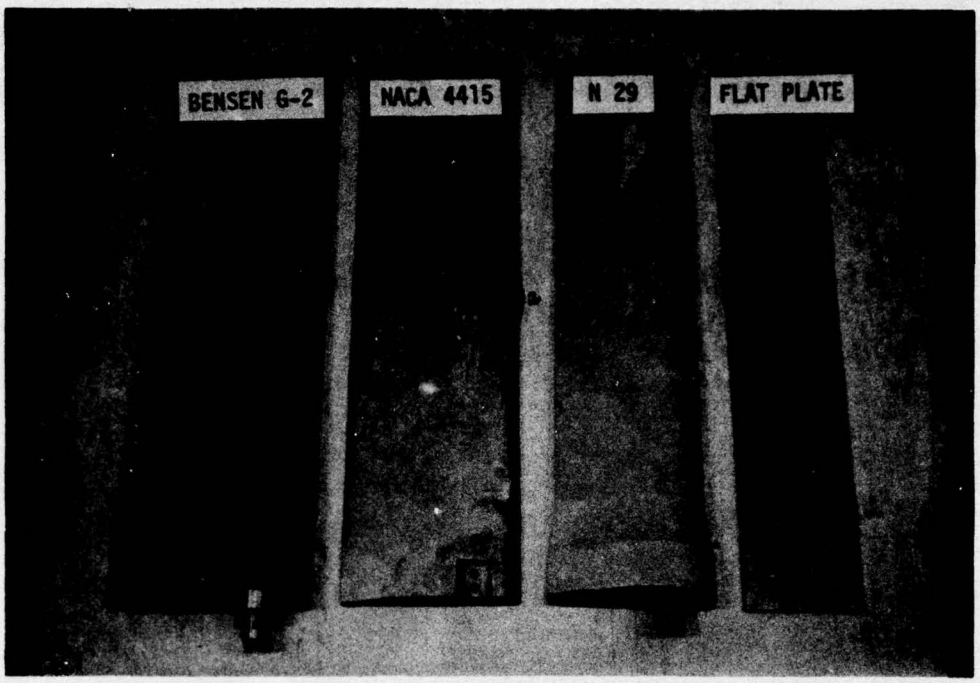

FIGURE 7. Planform View of Wing Models

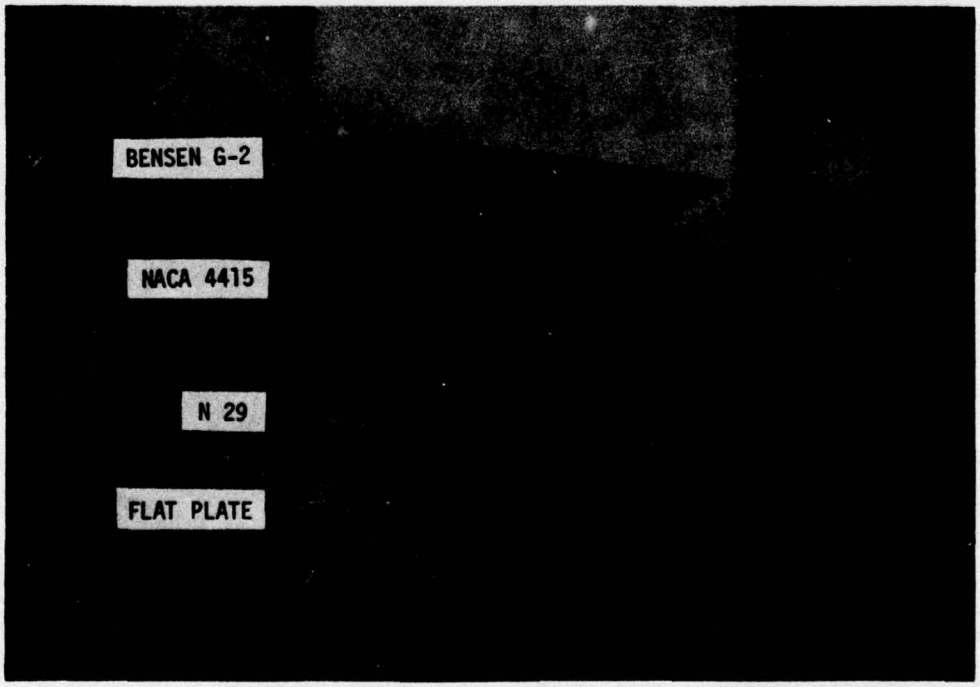

FIGURE 8. Wing Model Airfoil Sections

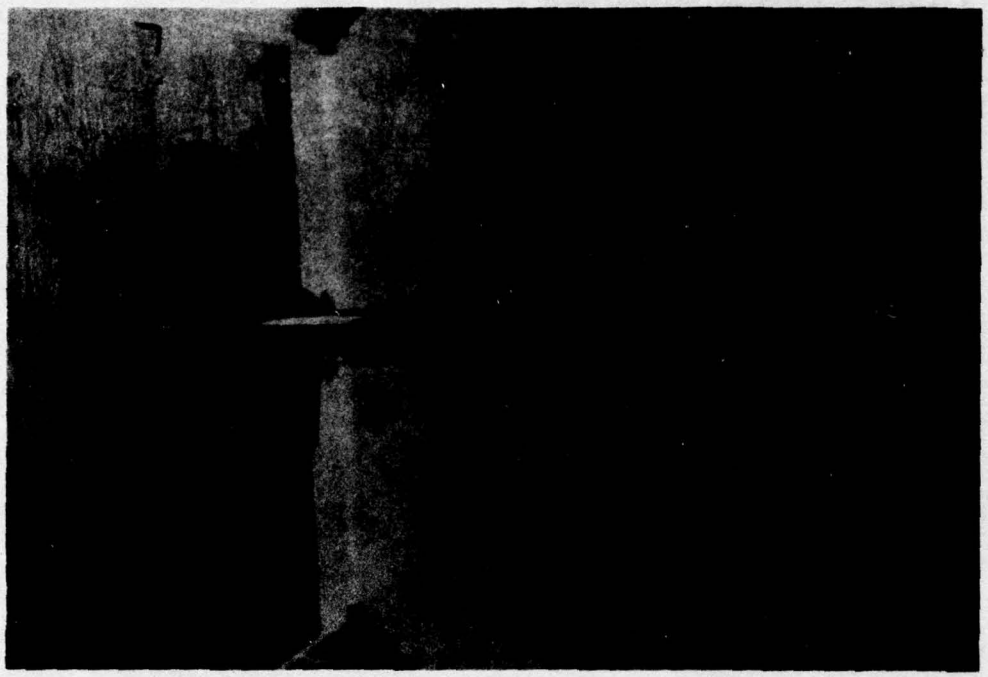

FIGURE 9. NACA 2415 Pressure Distribution Wing Model

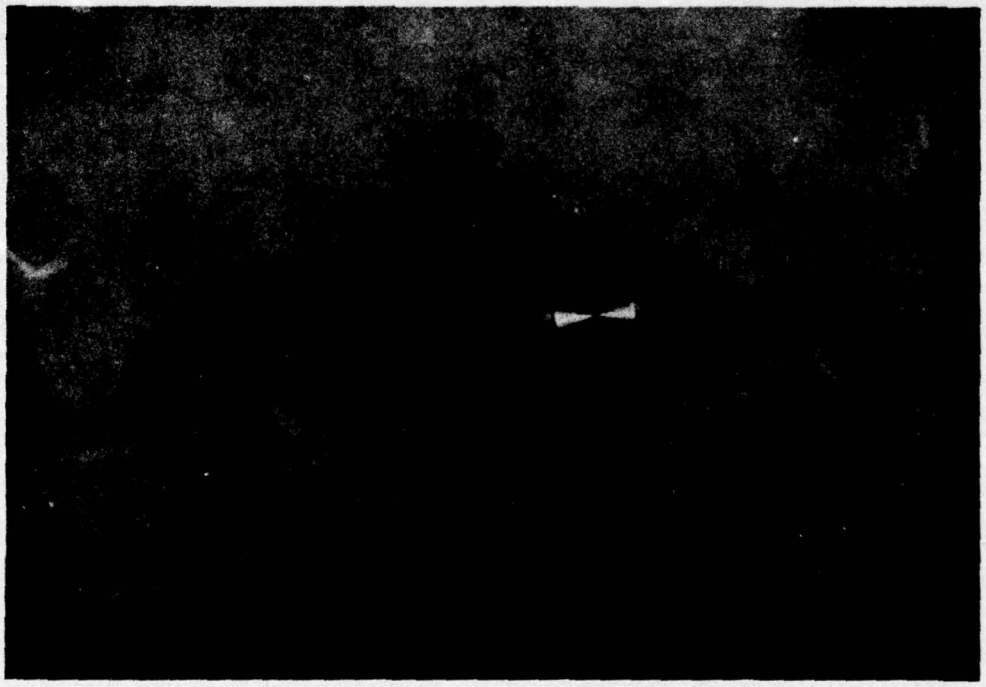

FIGURE 10. NACA 2431 Fairing for N29 Wing Mount

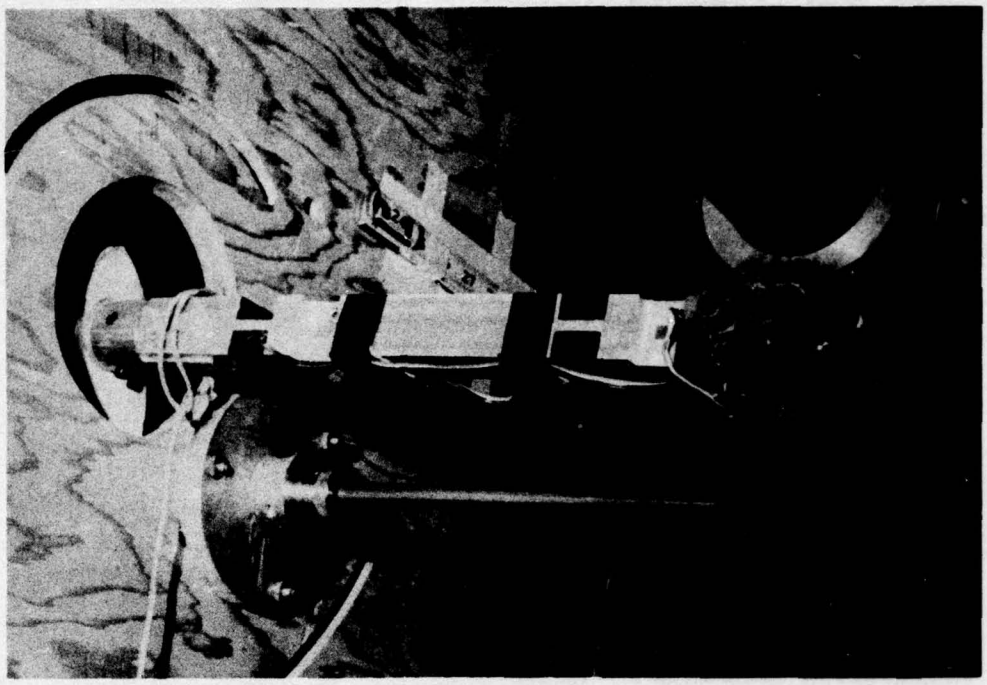

FIGURE 11. Four-Component Wing Strain-Gage Force-Balance

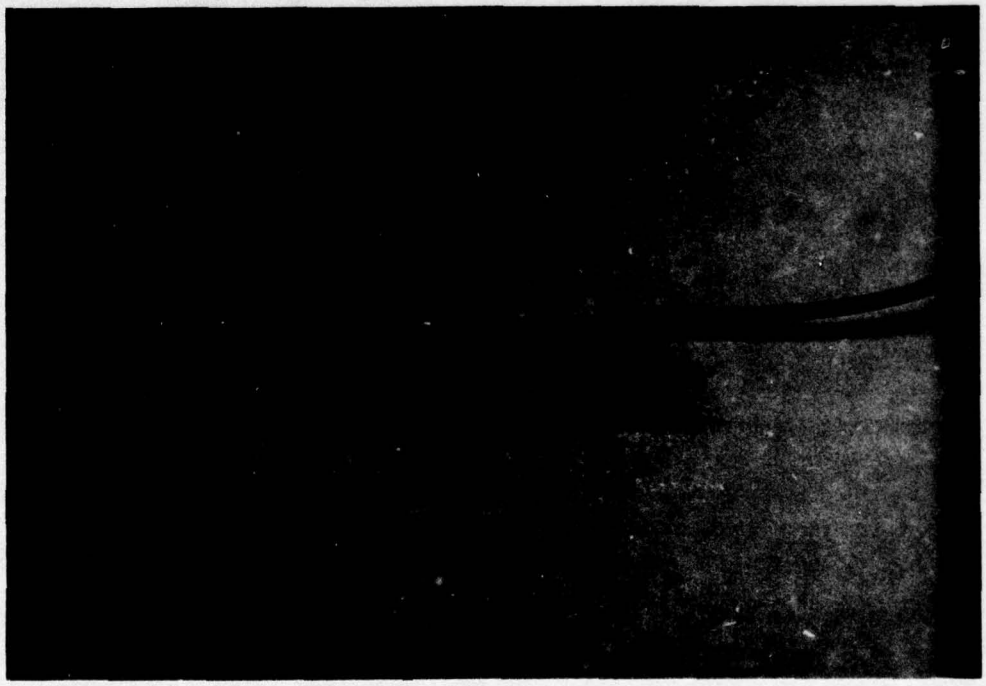

FIGURE 12. Two-Component Proprotor Strain-Gage Force-Balance

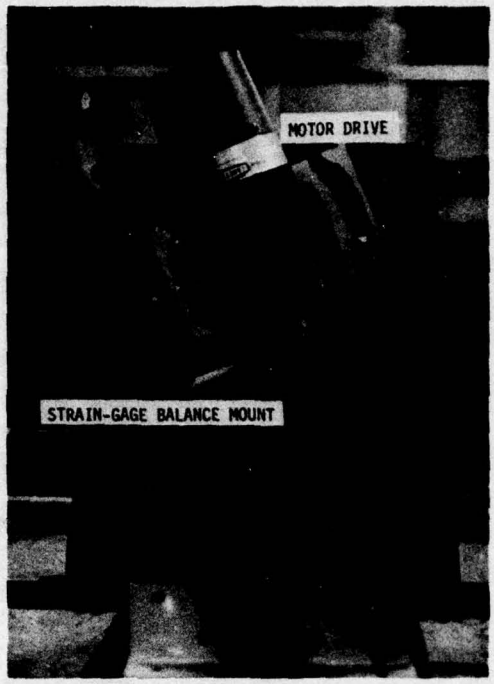

FIGURE 13. Proprotor Force-Balance Mount and Alignment System

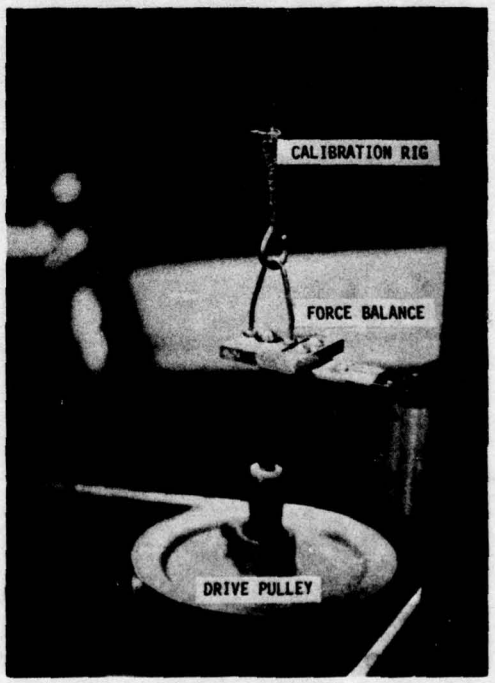

FIGURE 14. Proprotor Strain-Gage Force-Balance

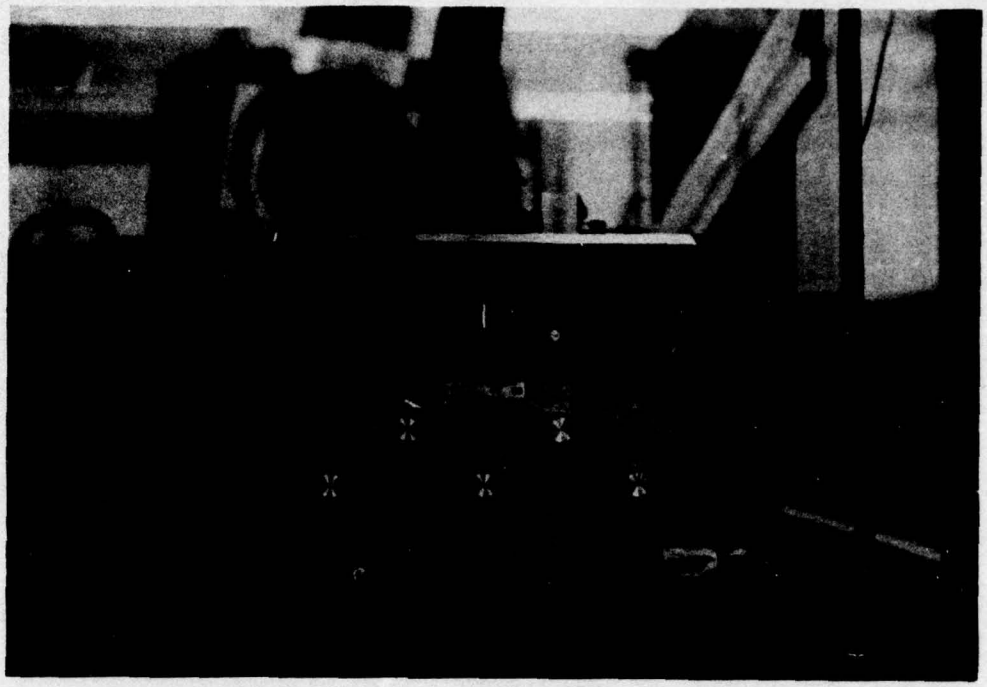

FIGURE 15. Vishay/Ellis-20 Strain Gage Indicator

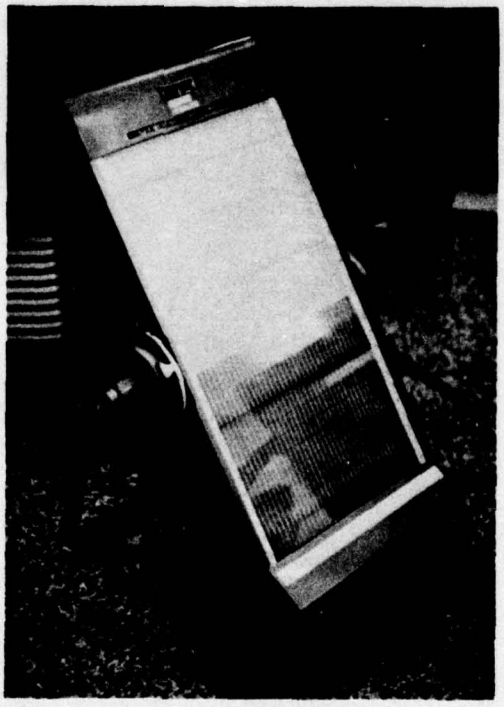

FIGURE 16. Multiple Bank Inclined Manometer

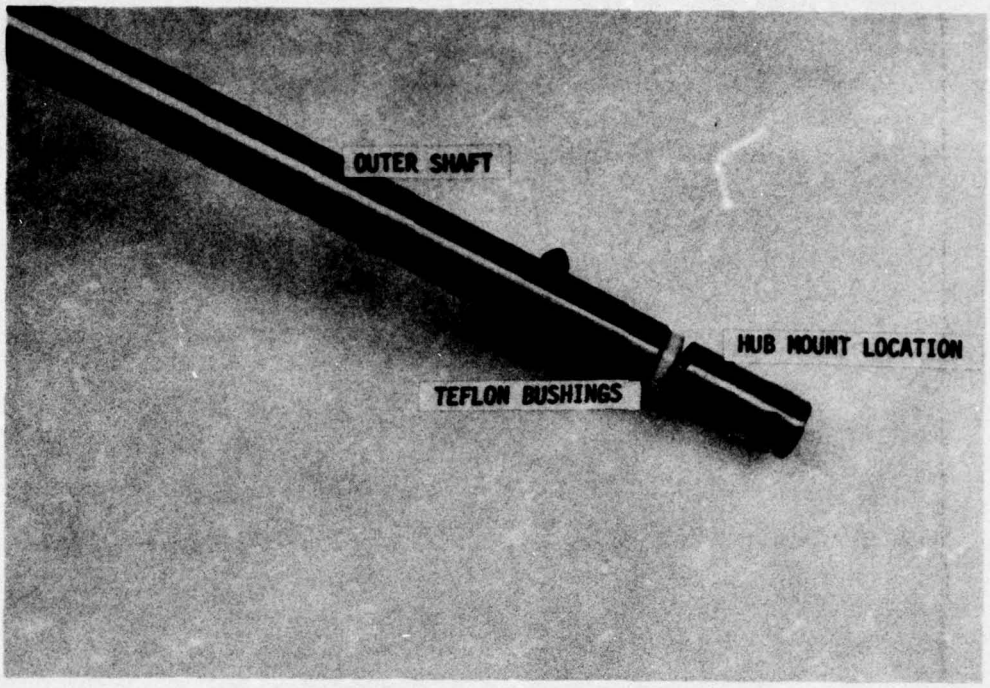

FIGURE 17. Proprotor Shaft Assembly

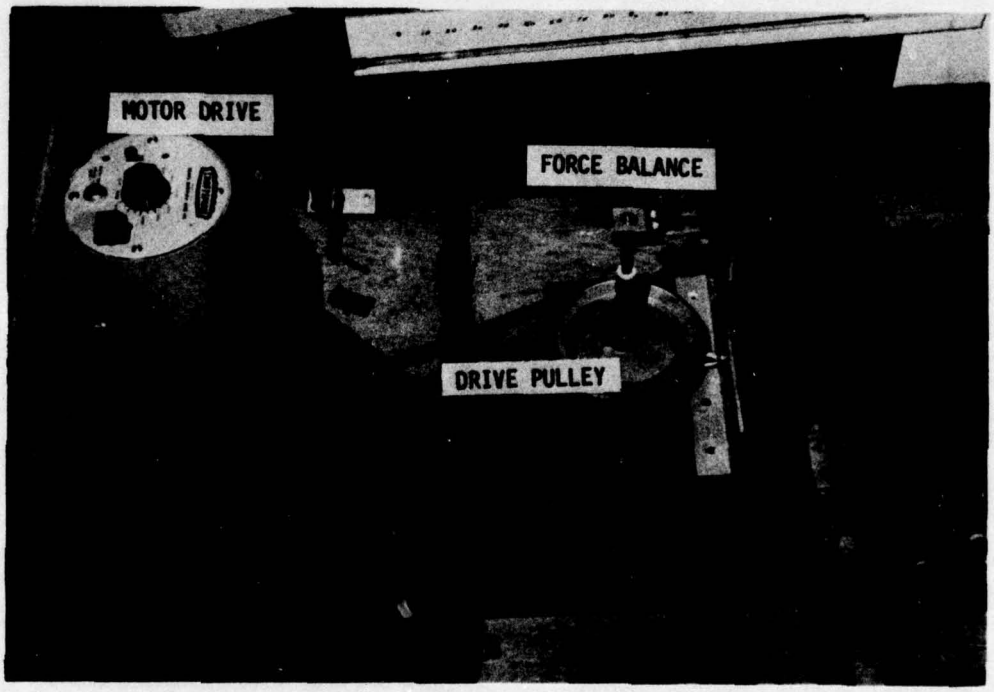

FIGURE 18. Proprotor Drive and Alignment Assembly

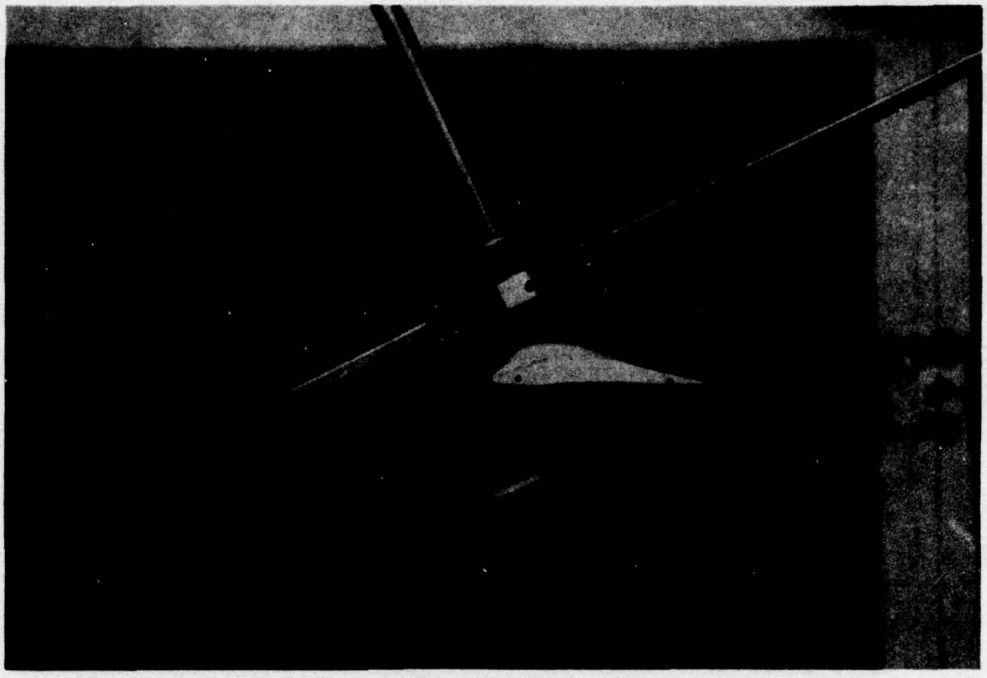

FIGURE 19. Orientation for Positive Proprotor Tilt Angle

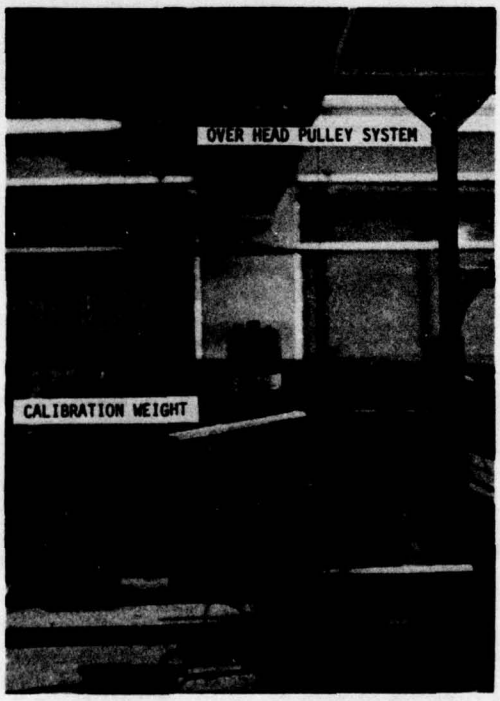

FIGURE 20. Pulley System for Proprotor Force Balance Calibration

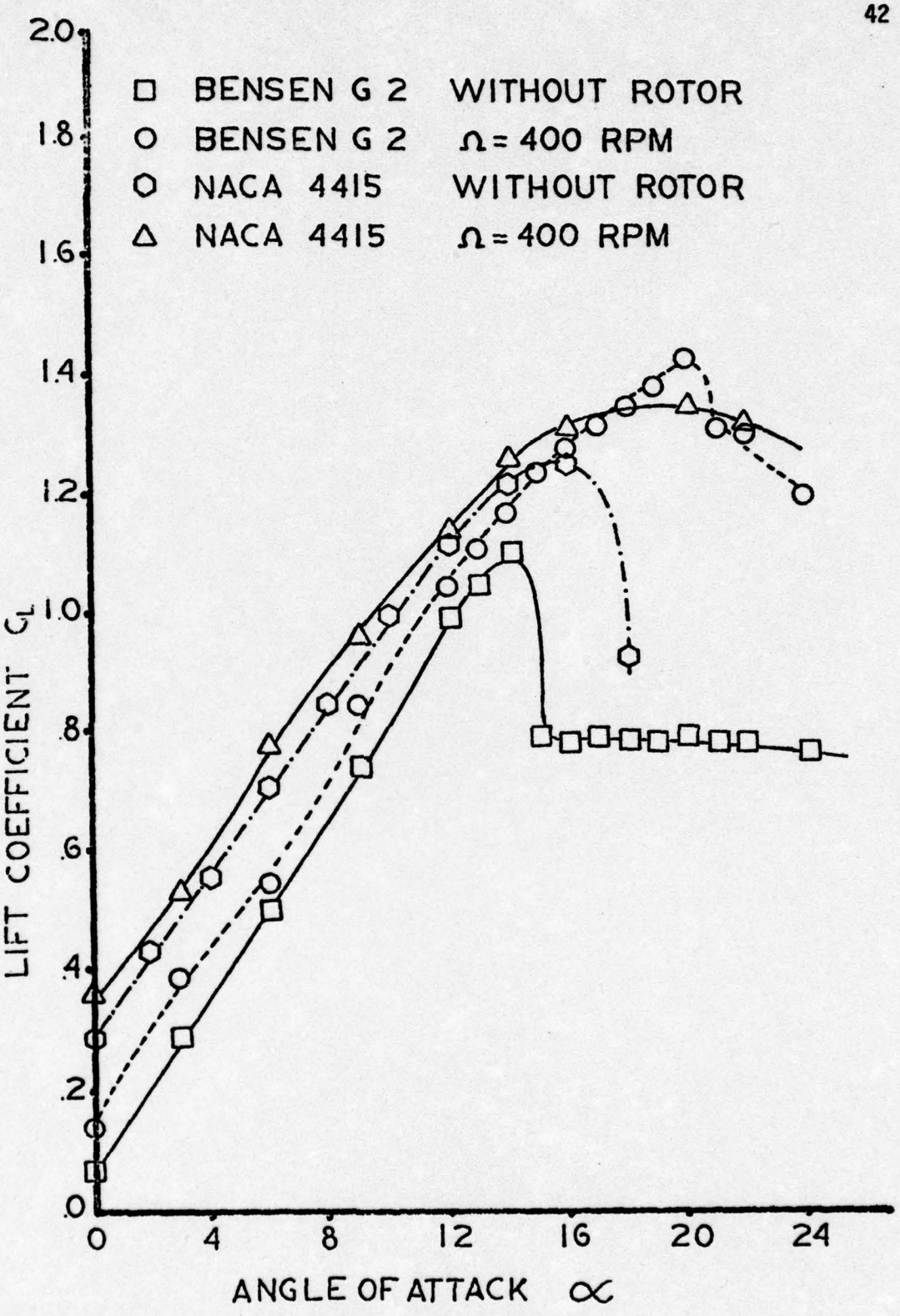

FIGURE 21 EFFECT OF PROPROTOR ON THE LIFT COEFFICIENT OF A BENSEN G-2 AND NACA 4415 WING

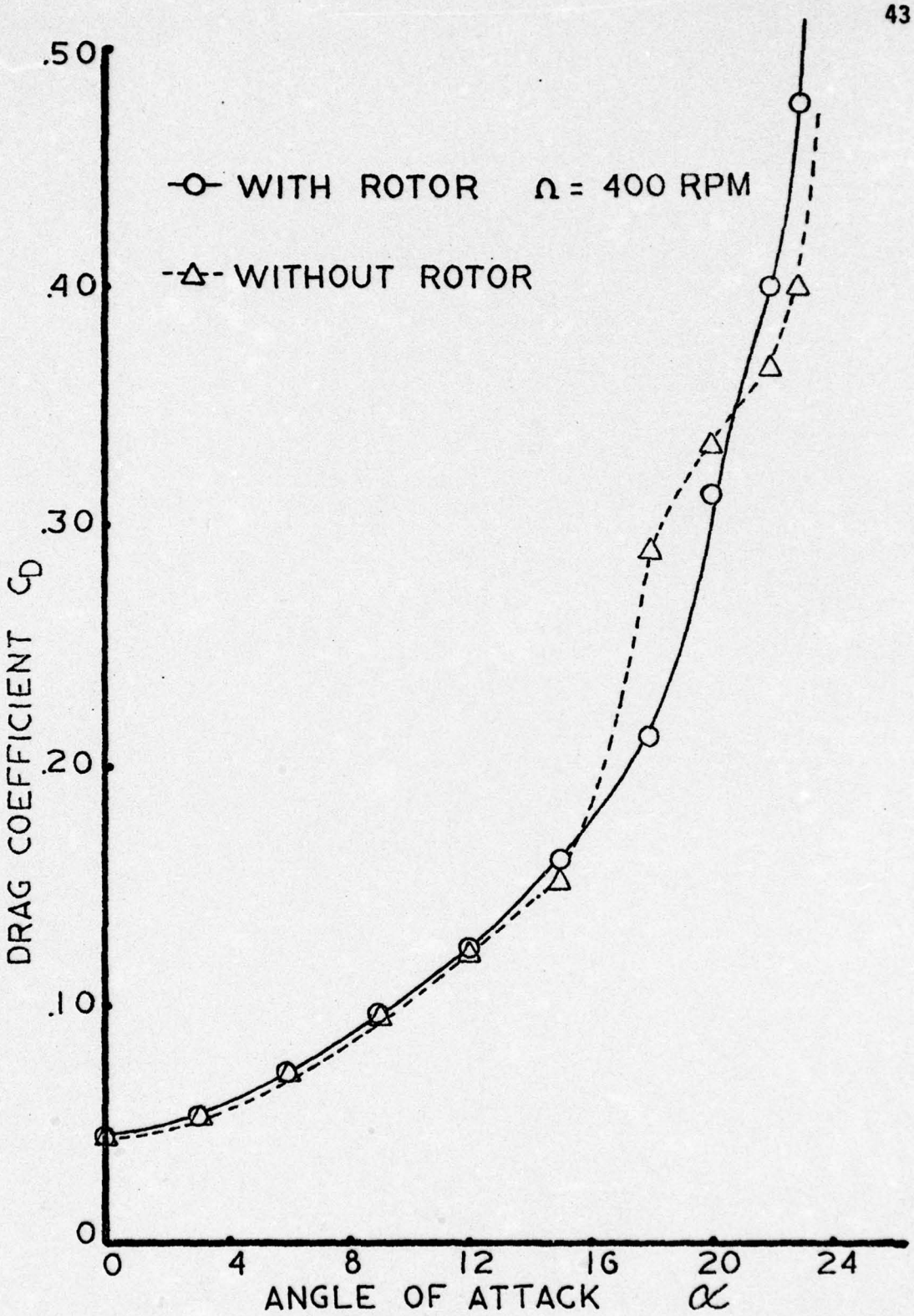

FIGURE 22 EFFECT OF PROPROTOR ON THE DRAG COEFFICIENT OF AN NACA 4415 WING

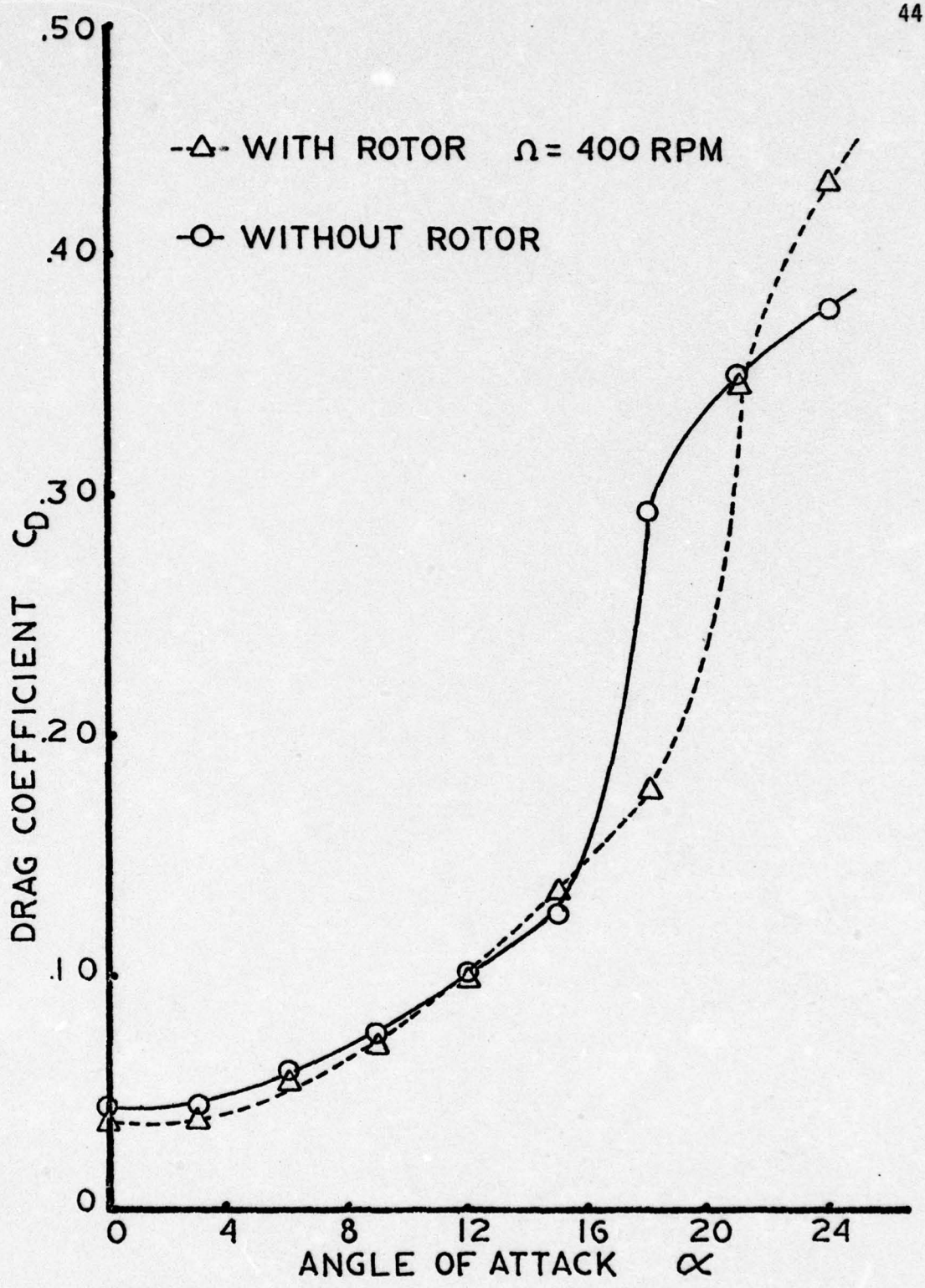

FIGURE 23 EFFECT OF PROPROTOR ON THE DRAG COEFFICIENT OF A BENSEN G-2 WING

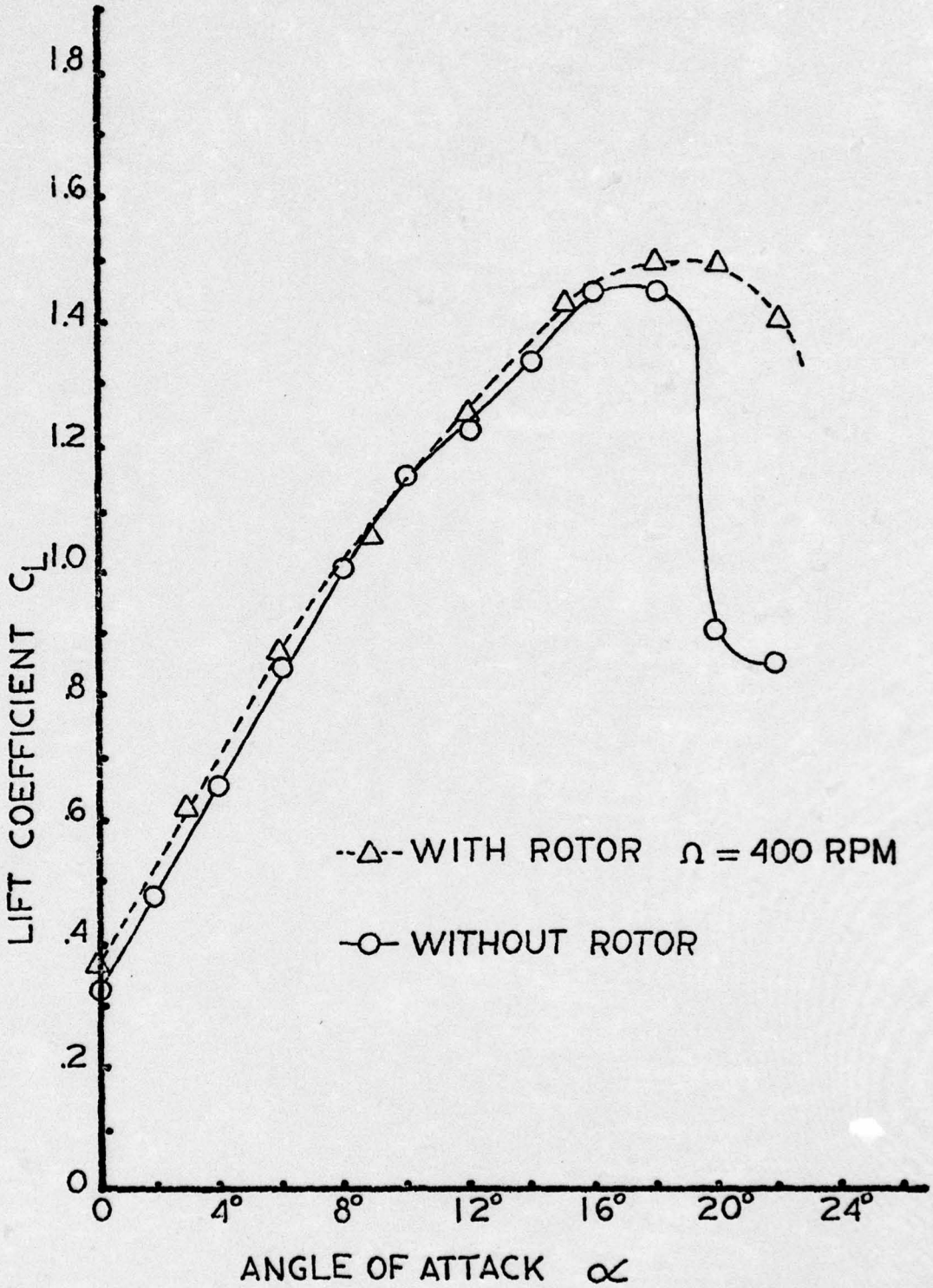

FIGURE 24 EFFECT OF PROPROTOR ON THE LIFT COEFFICIENT OF AN N29 WING

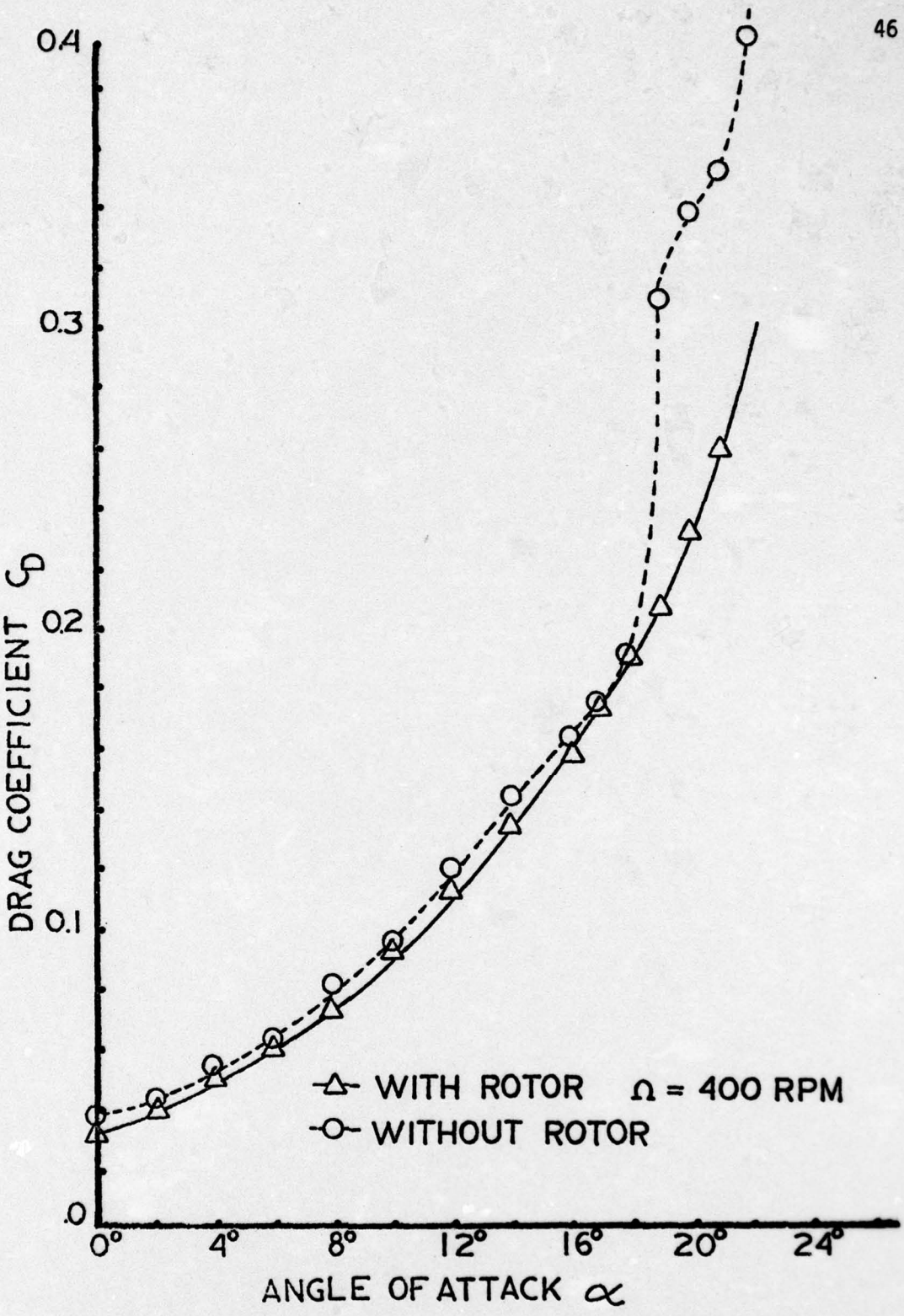

FIGURE 25 EFFECT OF PROPROTOR ON THE DRAG COEFFICIENT OF AN N29 WING

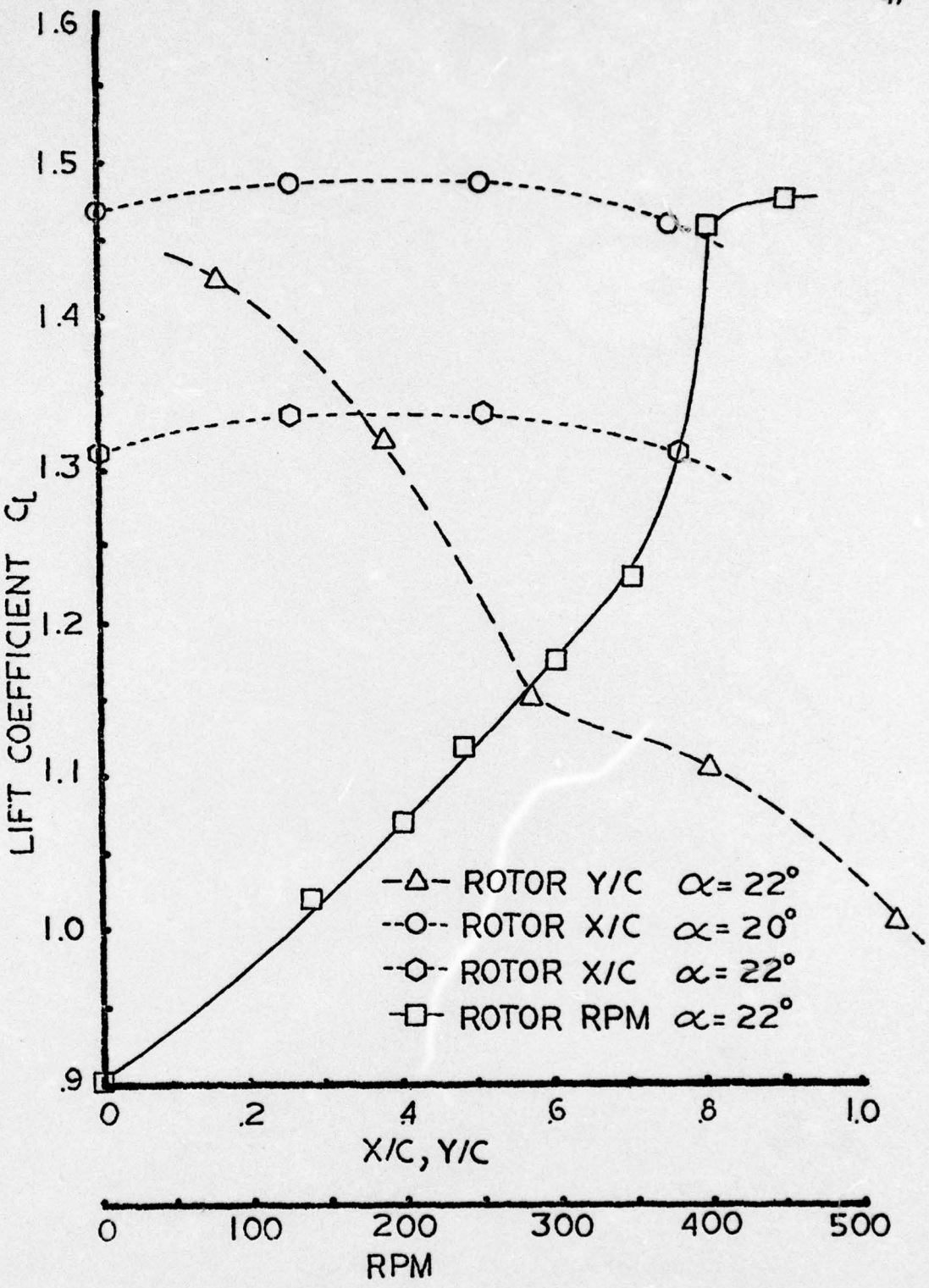

FIGURE 26 EFFECT OF PROPROTOR VARIABLES ON THE STALL LIFT COEFFICIENT OF AN N29 WING

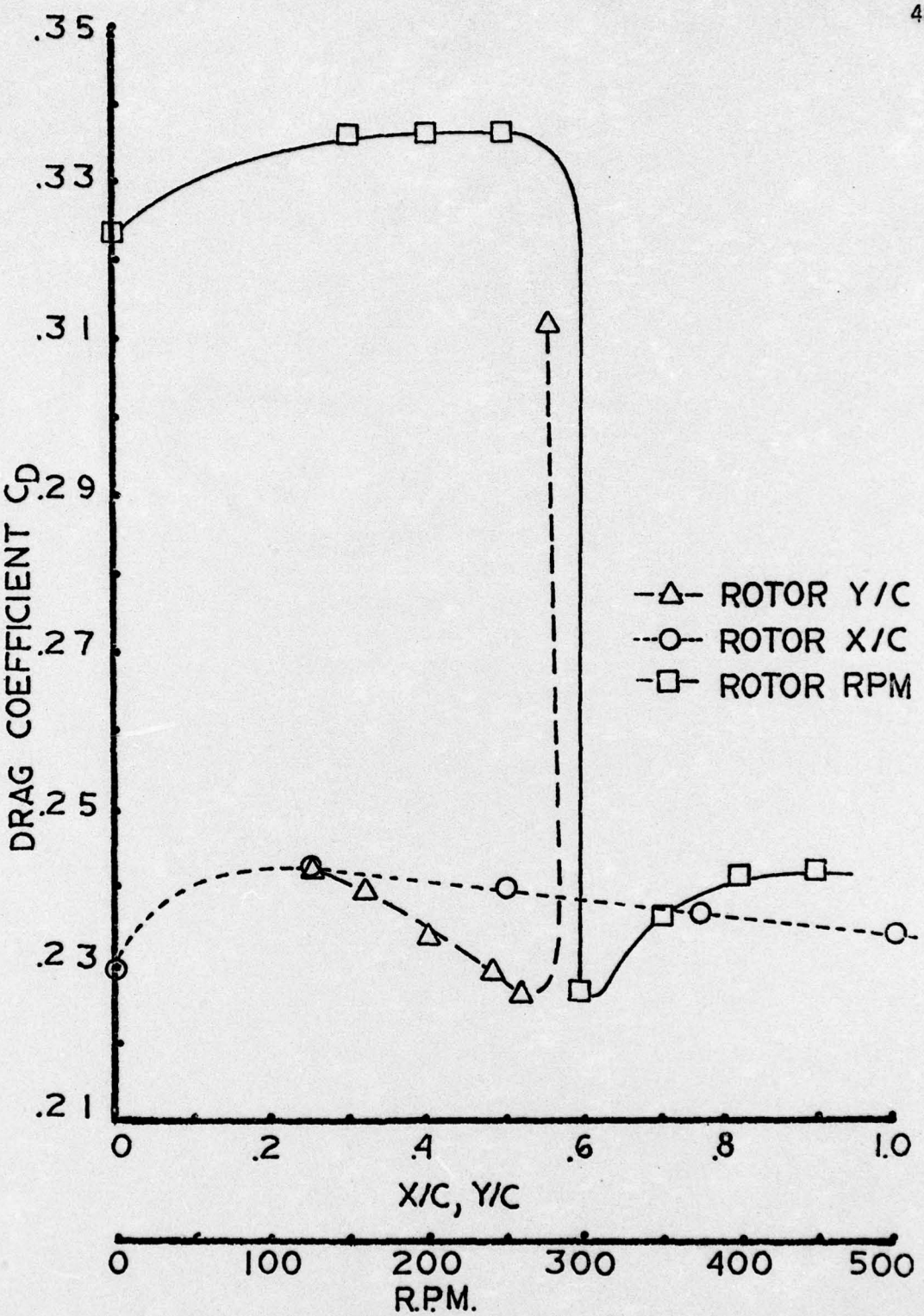

FIGURE 27 EFFECT OF PROPROTOR VARIABLES ON THE STALL DRAG COEFFICIENT OF AN N29 WING

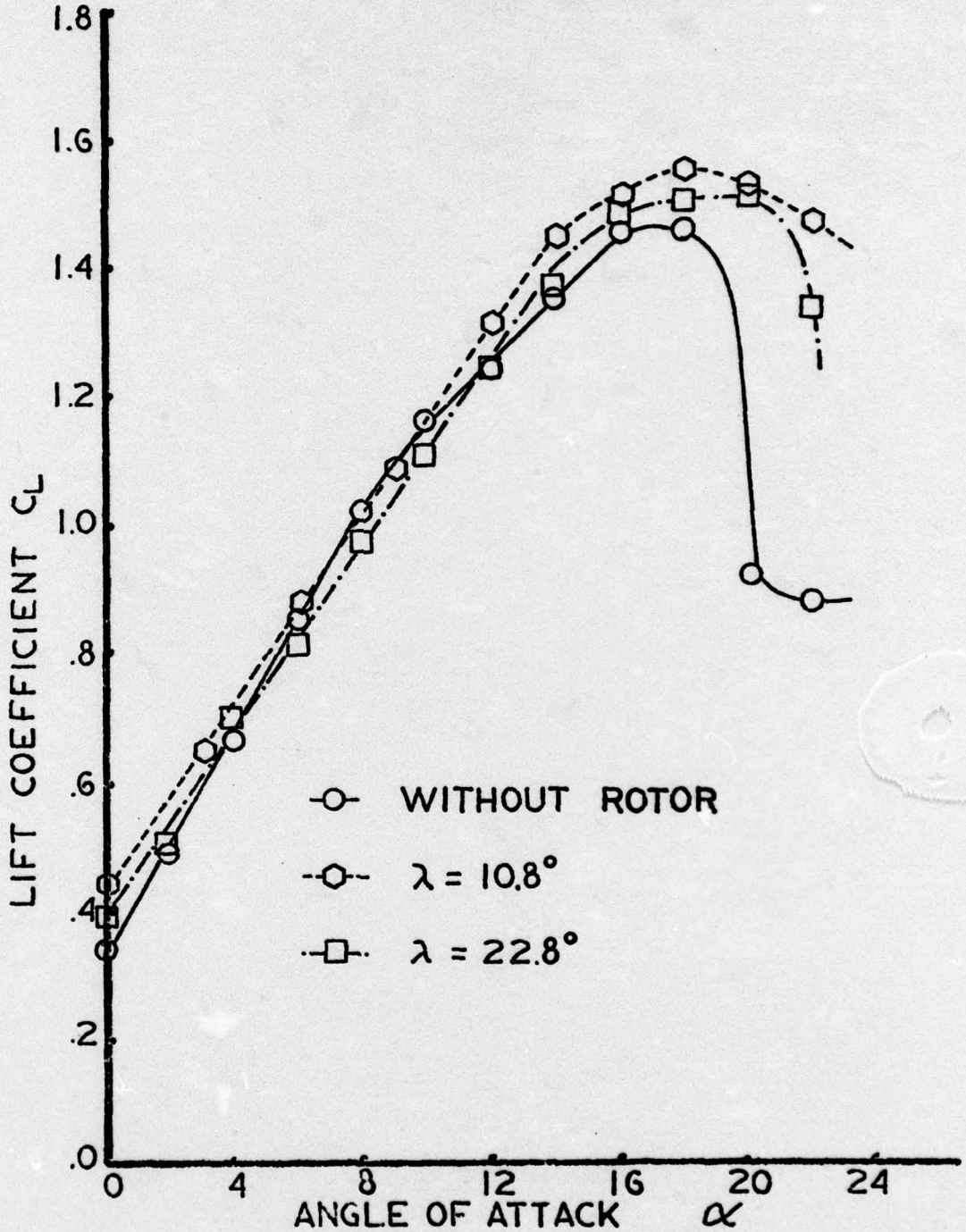

FIGURE 28 EFFECT OF PROPROTOR TILT ON THE LIFT COEFFICIENT OF AN N29 WING

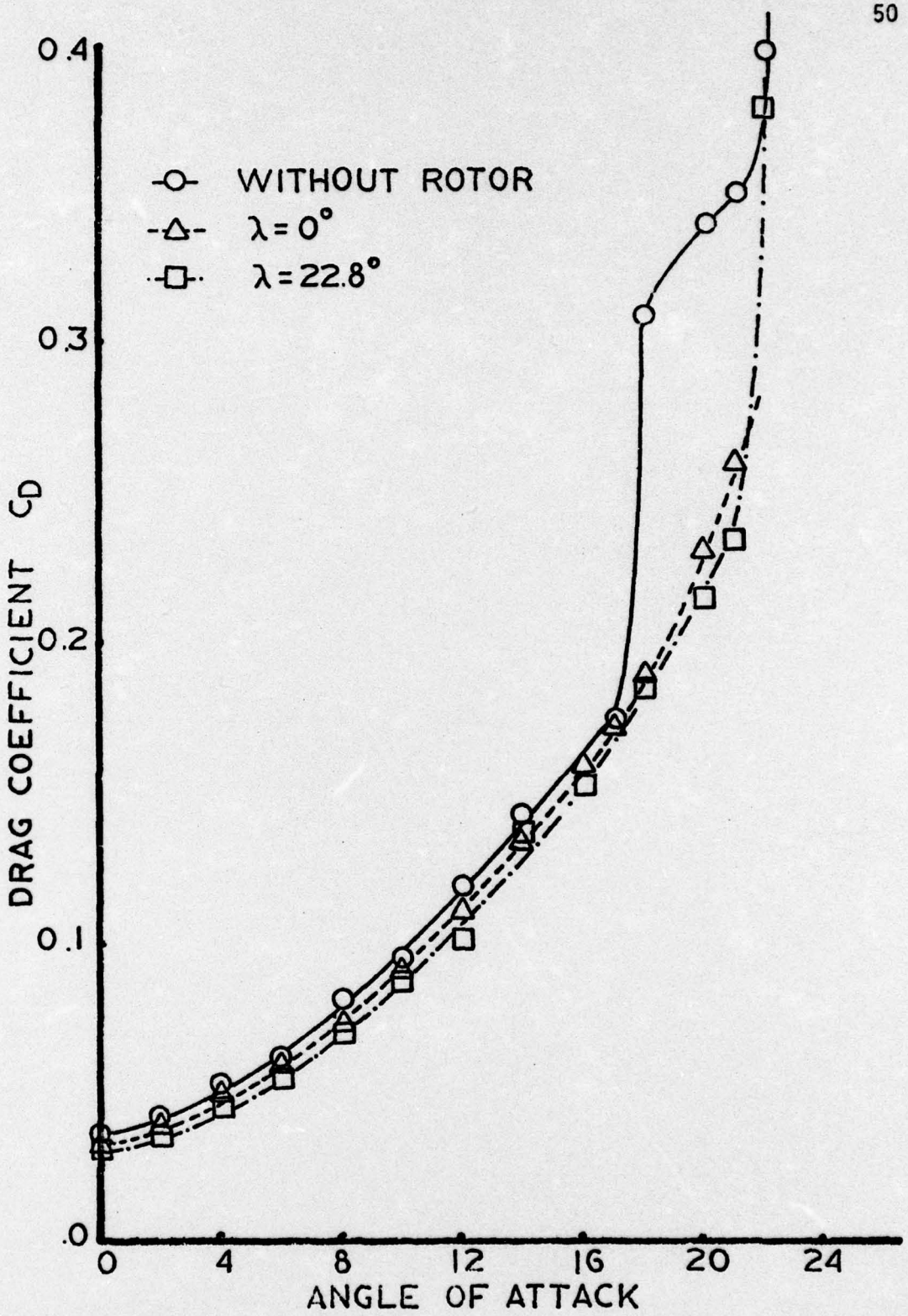

FIGURE 29 EFFECT OF PROPROTOR TILT ON THE DRAG COEFFICIENT OF AN N29 WING

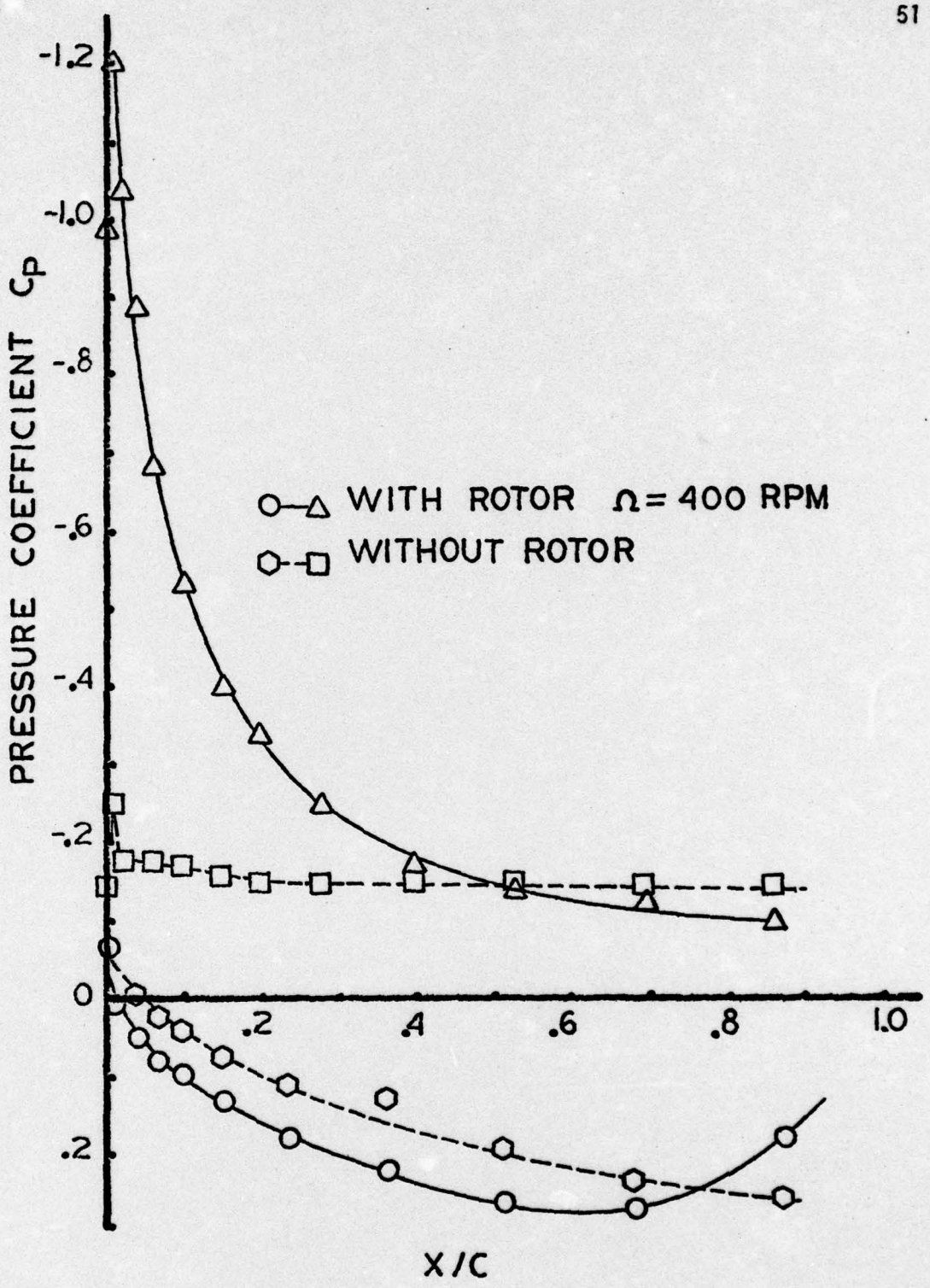

FIGURE 30 EFFECT OF PROPROTOR ON THE PRESSURE DISTRIBUTION OF AN NACA 2415 WING

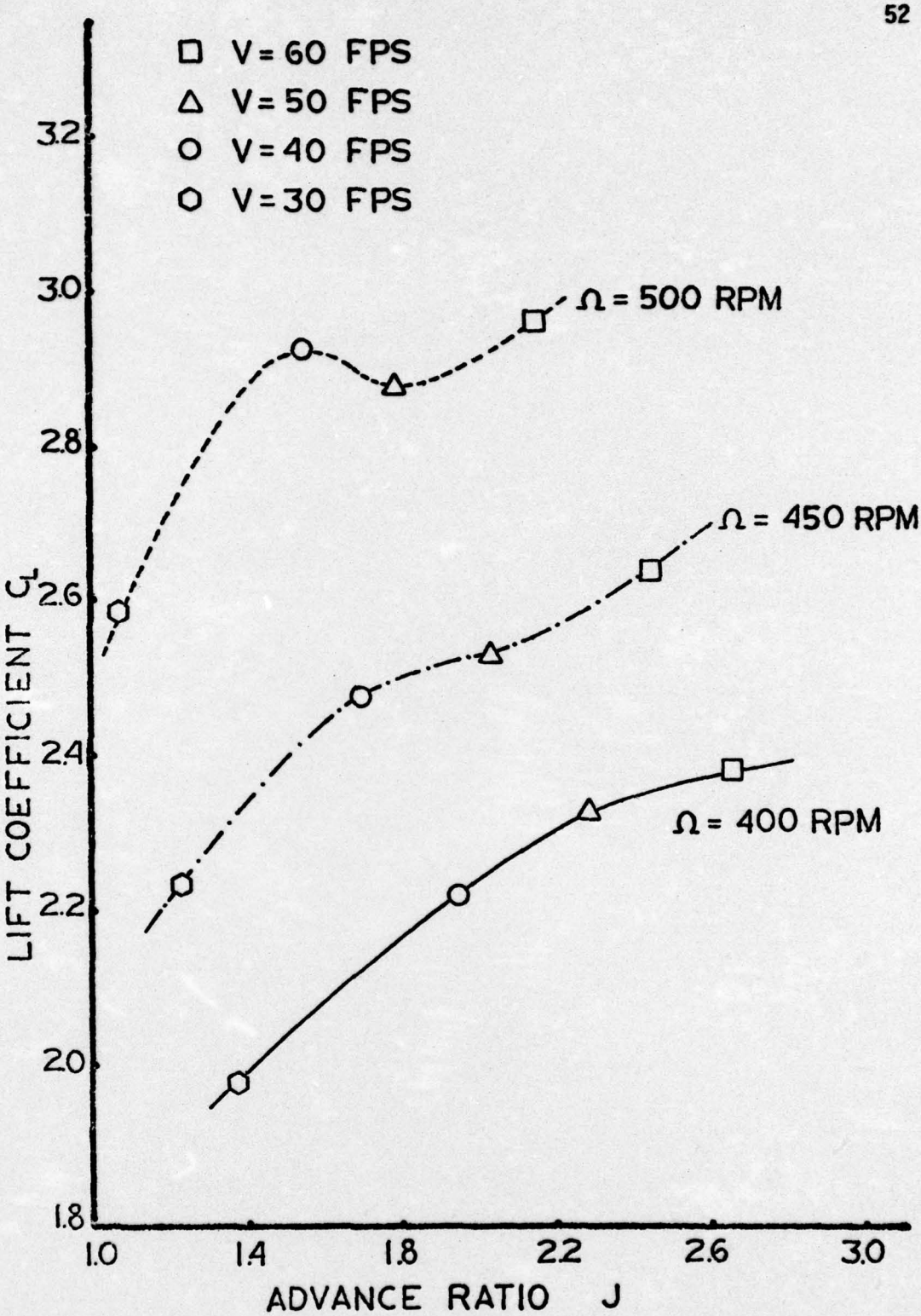

FIGURE 31 EFFECT OF ADVANCE RATIO ON THE PROPROTOR NONINTERFERENCE LIFT COEFFICIENT

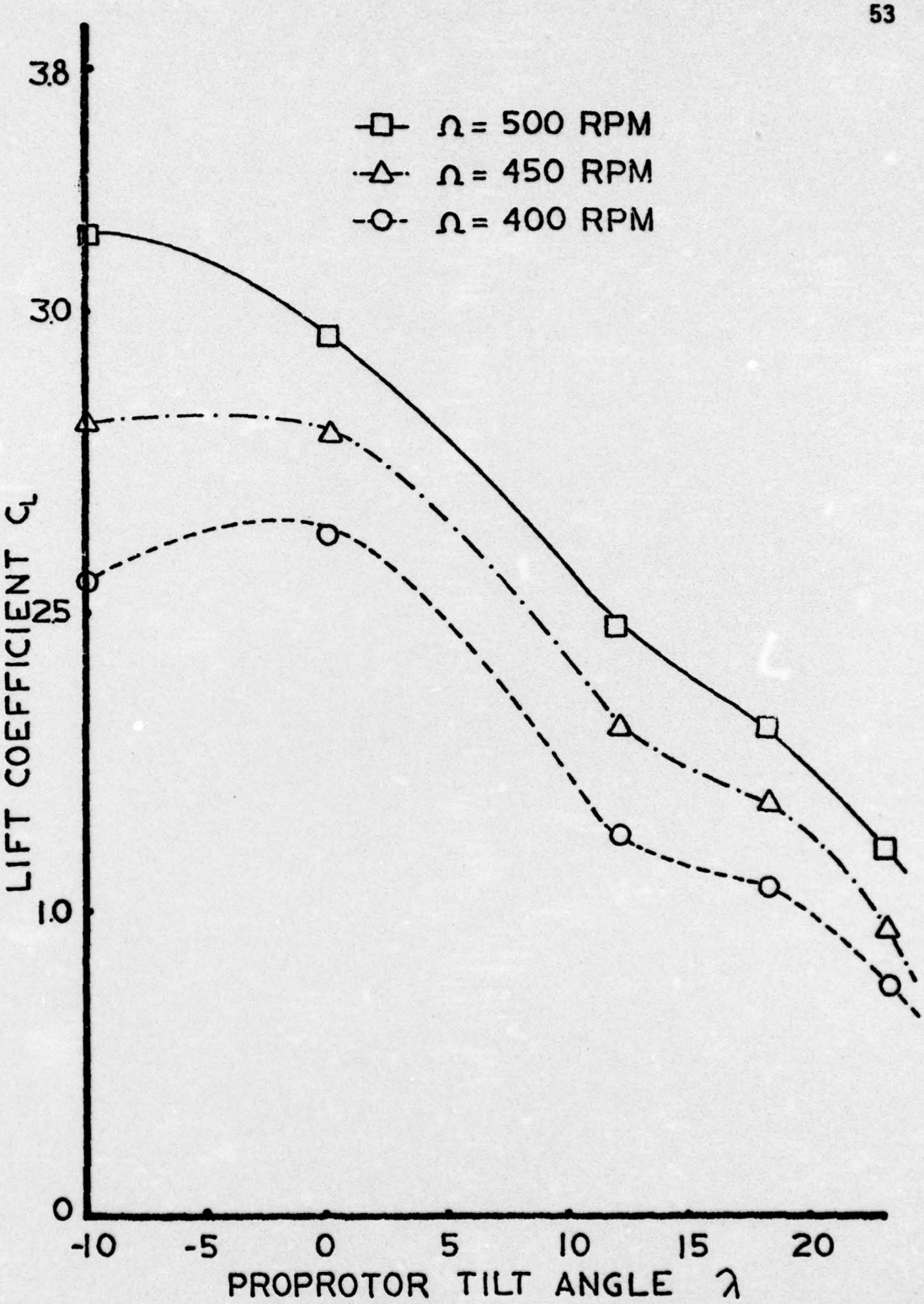

FIGURE 32 EFFECT OF TILT ANGLE ON THE PROPROTOR NONINTERFERENCE LIFT COEFFICIENT

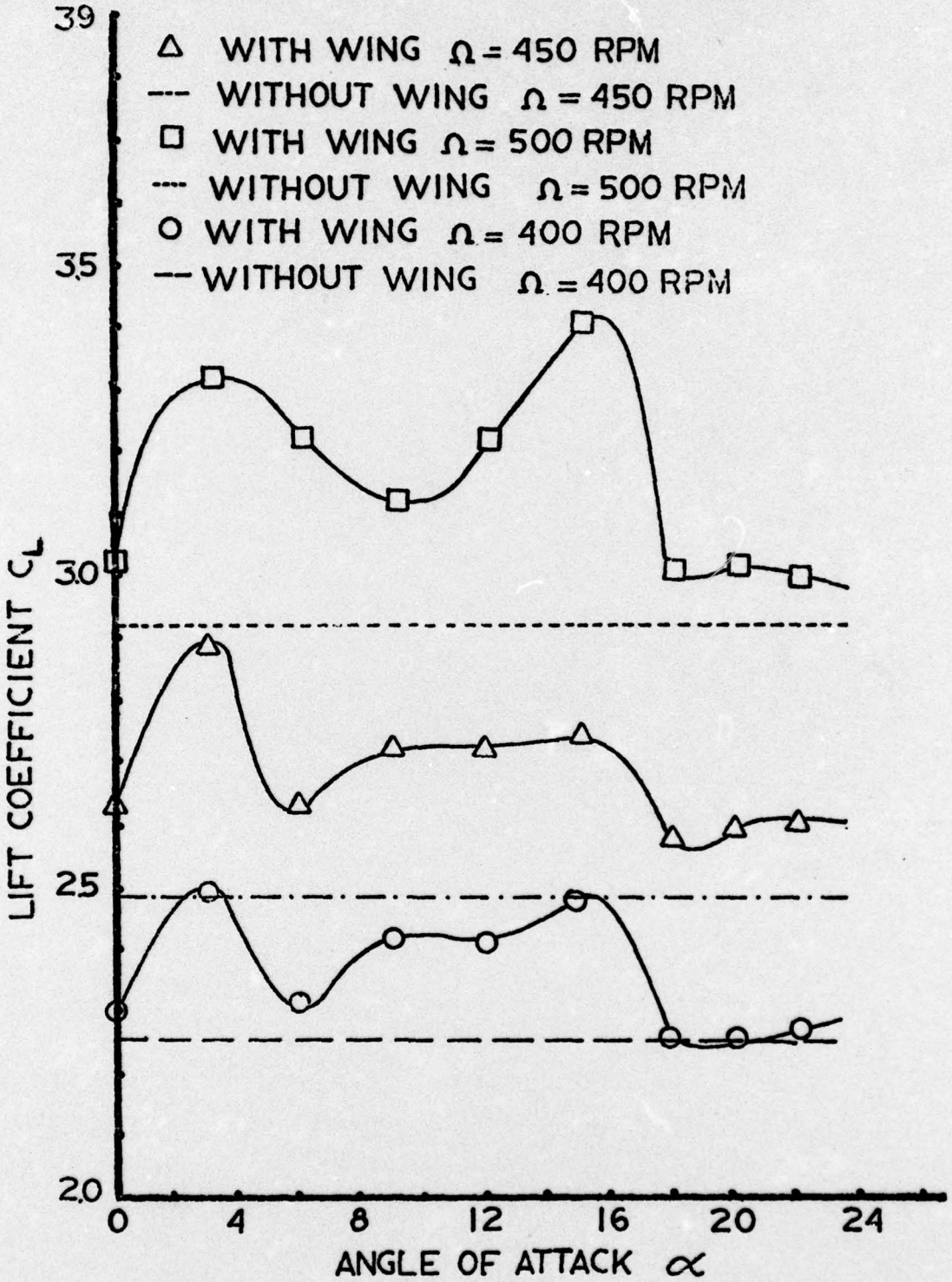

FIGURE 33 EFFECT OF WING INTERFERENCE ON PROPROTOR LIFT COEFFICIENT $\lambda = 0°$

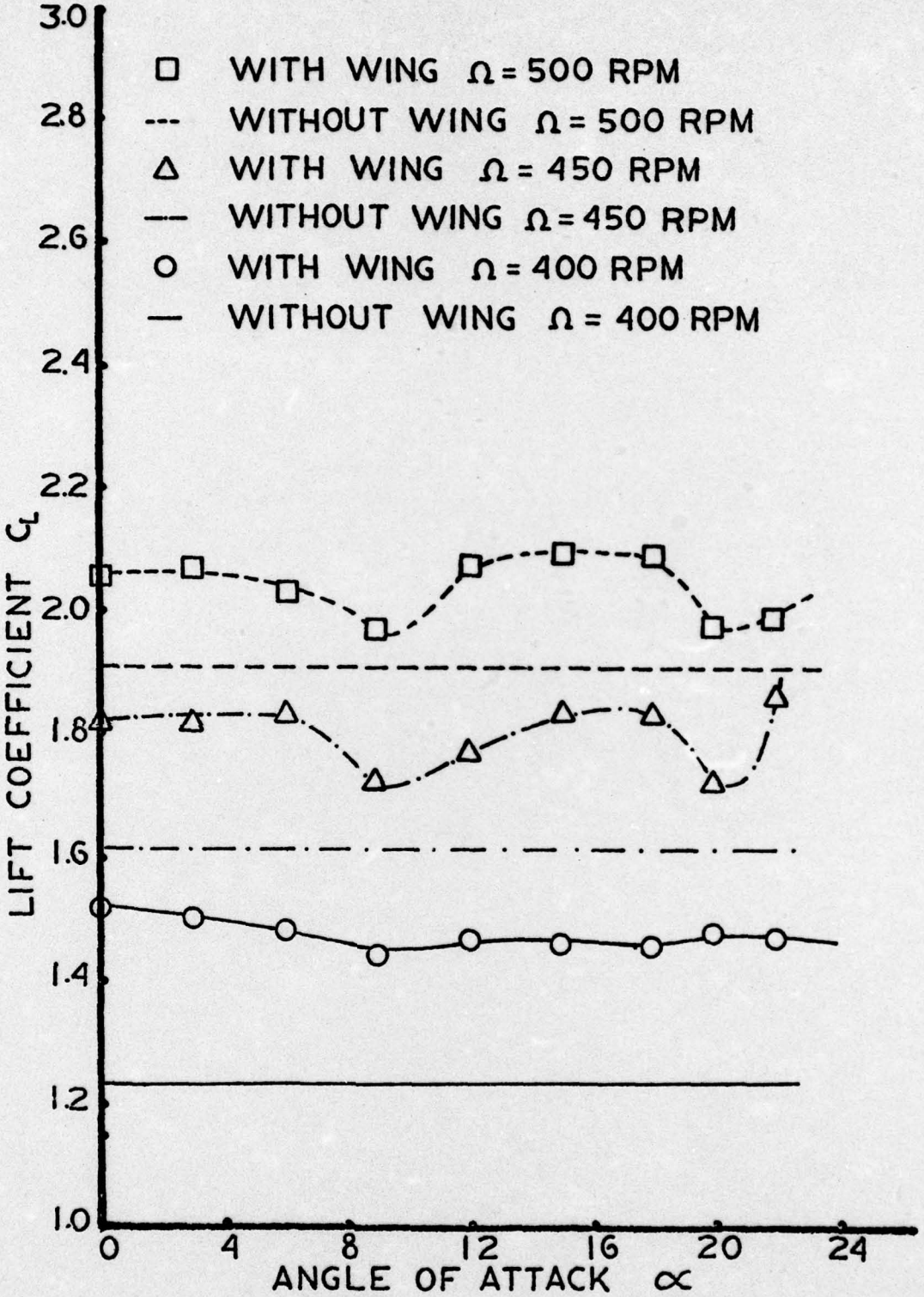

FIGURE 34 EFFECT OF WING INTERFERENCE ON PROPROTOR LIFT COEFFICIENT $\lambda = 10.8°$

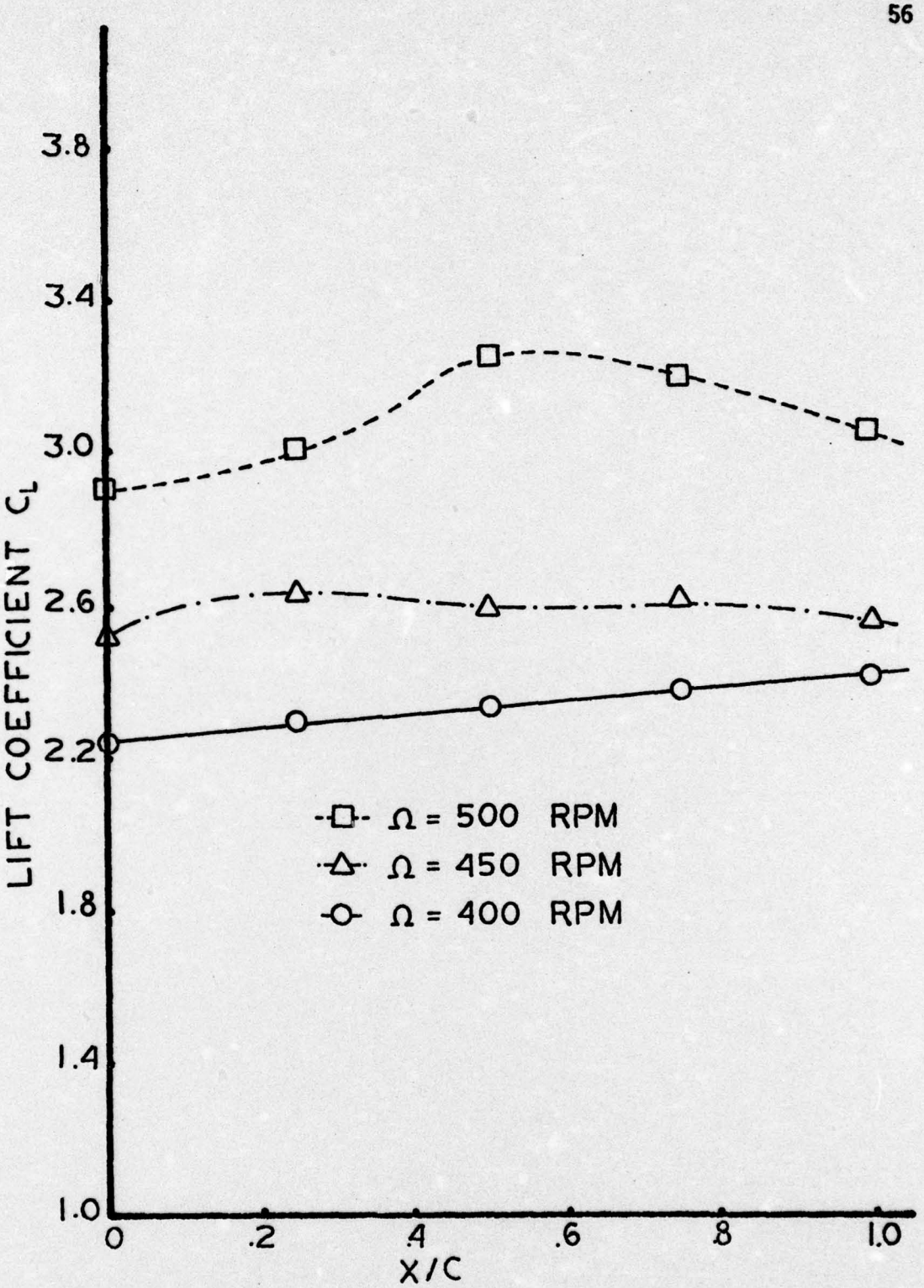

FIGURE 35 EFFECT OF PROPROTOR POSITION ON THE PROPROTOR LIFT COEFFICIENT

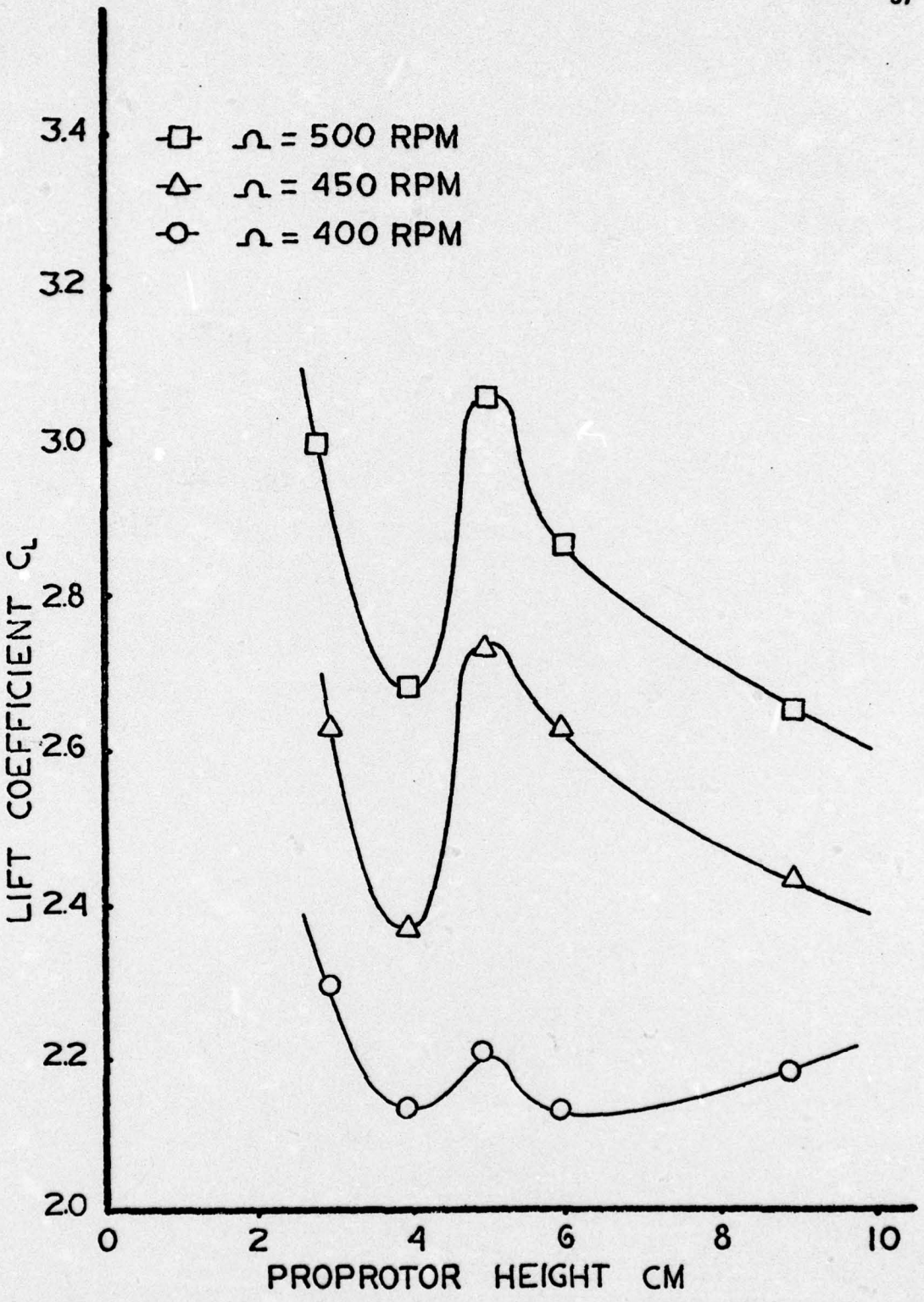

FIGURE 36 EFFECT OF PROPROTOR HEIGHT ON THE PROPROTOR LIFT COEFFICIENT

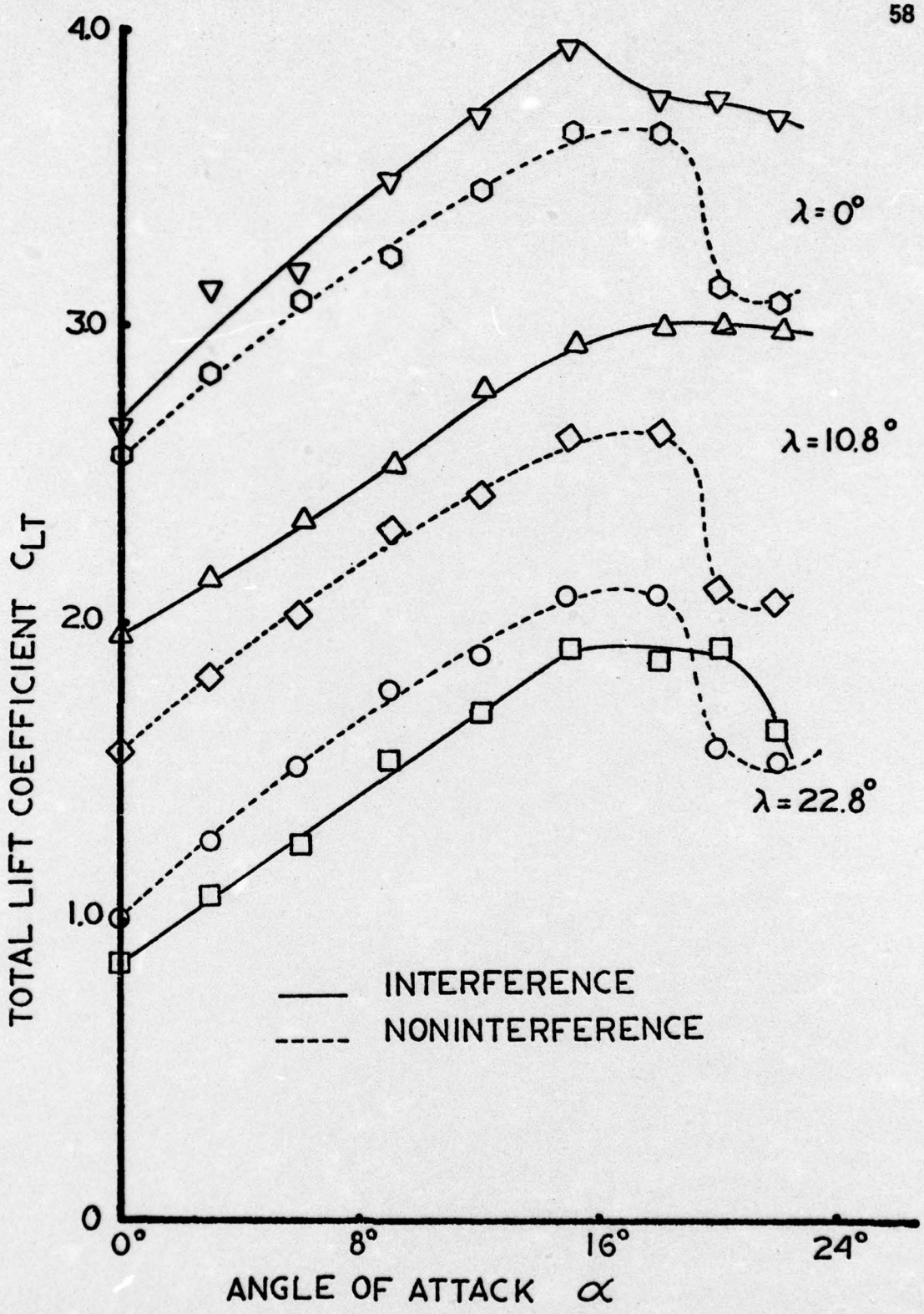

FIGURE 37 EFFECT OF INTERFERENCE ON THE TOTAL LIFT COEFFICIENT

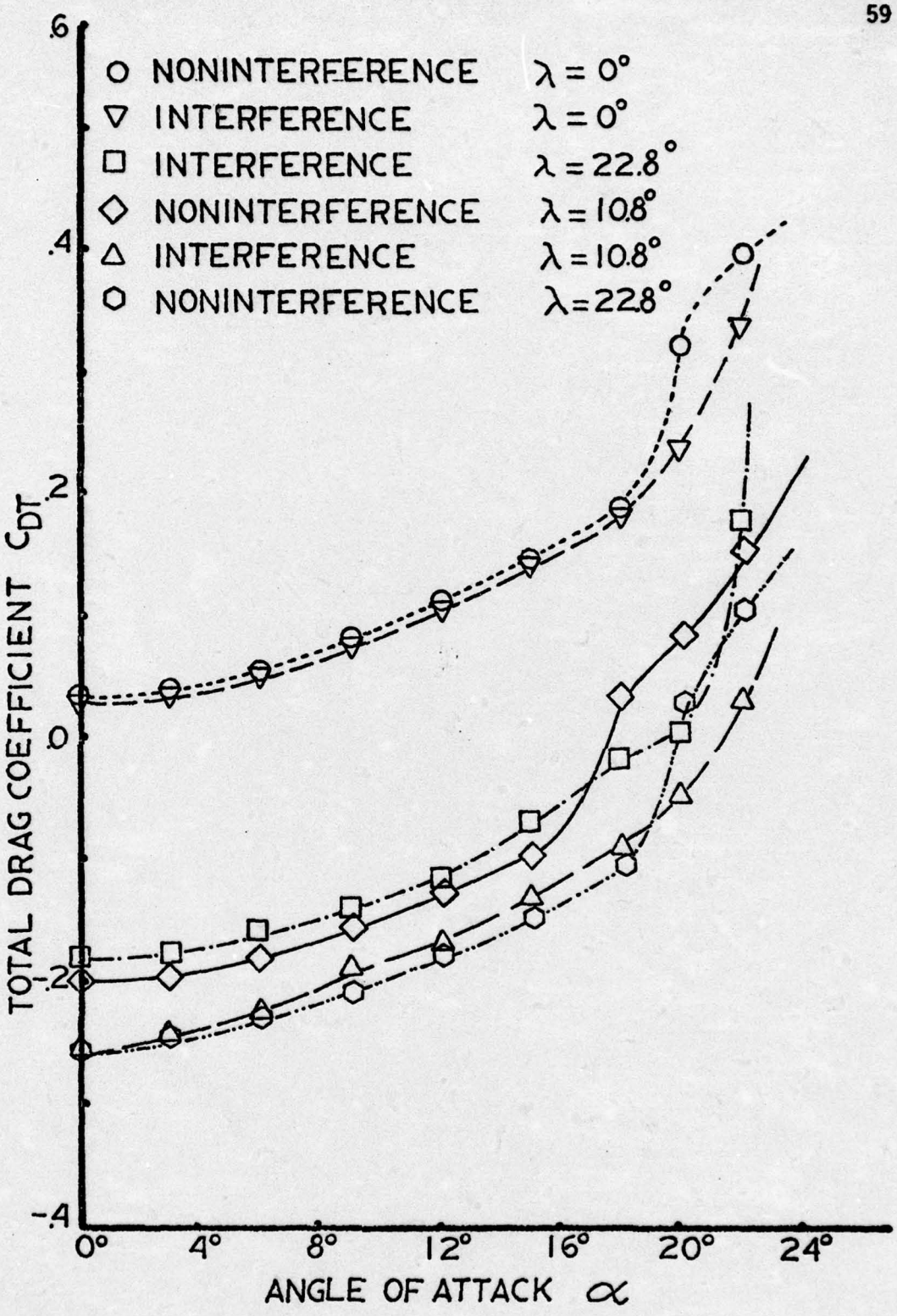

FIGURE 38 EFFECT OF INTERFERENCE ON THE TOTAL DRAG COEFFICIENT